Prepared for submission to JCAP

Future Parameter constraints from weak lensing CMB and Galaxy Lensing Power- and Bi-spectra

Jonas Frugte[1] **P. Daniel Meerburg**[1]

[1]Van Swinderen Institute for Particle Physics and Gravity, University of Groningen, Nijenborgh 4, 9747 AG Groningen, The Netherlands

E-mail: jonasfrugte@gmail.com, p.d.meerburg@rug.nl

Abstract. Upcoming Stage 4 surveys, such as the Simons Observatory, LSST, and Euclid are poised to measure weak gravitational lensing of the Cosmic Microwave Background (CMB) and galaxies with unprecedented precision. While the power spectrum is the standard statistic used to analyze weak lensing data, non-Gaussianity induced by the non-linear growth of structure imparts significant cosmological information into higher-order statistics. In this paper, we forecast the ability of future surveys to constrain cosmological parameters using the weak lensing power spectrum and bispectrum from both CMB and galaxy surveys, as well as their cross-correlations. We consider an eight-parameter cosmological model (ΛCDM + $\sum m_\nu$ + w_0) and assess parameter constraints for Stage 4 survey specifications. Our analysis shows that, in the absence of systematics, both the CMB and galaxy lensing bispectra will be detectable at high signal-to-noise. We consider parameter constraints with a "weak" prior and with a stronger prior from the primary CMB anisotropies. In the weak prior case the lensing bispectrum substantially improves parameter constraints over using the lensing power spectrum alone, primarily by breaking parameter degeneracies. For the stronger prior we see less significant gains, particularly for the CMB lensing bispectrum. We further find that for stage 4 surveys that are able to measure lensing on small scales where non-linear structure formation becomes important, the constraining power of the lensing bispectrum can become comparable to that of the lensing power spectrum. Furthermore, we demonstrate that, both for our weak and strong priors, the synergy between CMB and galaxy lensing is substantial. Combining the two probes, particularly with both their lensing power- and bi-spectra, leads to significantly tighter constraints than achievable with either probe individually, with the greatest improvement seen for the sum of neutrino masses. Additionally, we also analyze the changes in detectability and parameter constraints when taking into account post-Born corrections to the lensing bispectra, as these were shown to be significant, especially for the CMB lensing bispectrum [31]. We show that the conclusions of this paper remain largely the same with this correction.

Contents

1 Introduction

Weak lensing has been used as a probe to constrain cosmological parameters for over a decade [23, 4, 20, 37, 5, 30]. A range of upcoming surveys, such as the survey by the Simons Observatory (SO) [2], the Legacy Survey of Space and Time (LSST) [18], and Euclid [24] aims to measure weak lensing of the cosmic microwave background (CMB) and galaxies respectively. These upcoming surveys are expected to achieve significantly higher accuracy than their predecessors, leading to tighter

constraints on cosmological parameters and advancing our overall understanding of cosmology. Typically, the standard summary statistic of interest is the power spectrum (or equivalently, two-point function) of the lensing potential (as well as cross-correlations with galaxy clustering). This can be measured in terms of the lensing convergence κ, lensing shear γ, or lensing potential ψ. In the weak lensing regime and under the Born approximation they are all equivalent, in the sense that they can be directly converted into one another (appendix B). In CMB surveys, the temperature and polarization anisotropies are used to reconstruct the lensing potential [17], while with galaxies one instead calculates lensing effects by measuring the lensing shear, which can be deduced from the ellipticity distribution of the observed galaxies [16].

Even with Gaussian initial conditions, there are significant amounts of non-Gaussianity in the weak lensing signal, especially in galaxy lensing due to it being a probe of the more recent distribution of matter [8, 35]. In addition to looking at the power spectrum, a natural next step is thus to measure weak lensing bispectra. While the bispectrum has been measured for galaxy lensing signals [38], a definitive detection of the CMB lensing bispectrum is still pending [22, 28]. Upcoming surveys, such as the ones mentioned earlier may be able to detect this signal. Therefore it is timely to consider the potential of higher order spectra to constrain cosmological parameters.

Additionally, we will also look at the effects of post-Born corrections. The CMB and galaxy lensing power spectra are typically affected by less than 1% [31, 33]. The galaxy lensing bispectrum is only affected by a few percent at most [7]. The only significant effect is on the CMB lensing bispectrum, as was shown in a 2024 paper [31]. In particular, for the folded configuration the effect can be of the same magnitude as the lensing bispectrum due to nonlinear large scale structure (2.2). It is thus worth considering how including first order corrections changes the detectability of the CMB lensing bispectrum and the associated parameter constraints. This analysis will shed light on whether or not the the Born approximation is still appropriate to use if one were to calculate and use the CMB lensing bispectrum using future data.

In this paper, we aim to answer these questions by adopting experimental parameters similar to those of next-generation surveys. We are especially interested in seeing if approximate parameter degeneracies can be broken by combining CMB and galaxy weak lensing power- and bi-spectra. We will consider ΛCDM parameters and extensions thereof. Of particular interest are the sum of neutrino masses $\sum m_\nu$ and dark energy equation of state parameter, w_0.

The structure of this paper is as follows: we introduce relevant formulas for weak lensing statistics, nonlinear matter bispectrum, and Fisher matrix formalism in section 2. We specify details such as the fiducial values of the parameters and noise models used in section 3. Parameter constraints and signal-to-noise ratios are presented in section 4 and discussed in section 5. Useful derivations relevant to this paper can be found in the appendices. In particular, they include a derivation for the Fisher matrix formalism for the non-trivial context of bispectra with multiple tracers.

All code used to derive the results in this paper is publicly available on GitHub at `https://github.com/Jonas-Frugte/fisher_calc_weak_lensing`.

2 Background

2.1 Weak lensing spectra

Radiation from cosmological objects is distorted due to gravitational lensing. Due to the low density of the cosmic web, the average deflection of a photon as it propagates through the universe is relatively weak. We thus work under the assumption that all deflection angles are small, this is referred to as the weak lensing regime. Weak lensing is quantified through the deflection field $\mathbf{d}(\hat{\mathbf{n}})$ which equals the difference between the observed angle of a point in the sky and the true (unlensed) angle. This field is the gradient of the lensing potential, $\psi(\hat{\mathbf{n}})$, which is expressed as a weighted integral of the mass distribution along the line-of-sight from the observer to the source.

In the case of CMB surveys, lensing alters the statistical properties of the temperature and polarization fields and can thus be calculated by comparing the observed signal to the expected unlensed signal (see e.g. [26, 27, 15]). In galaxy surveys, lensing alters the ellipticities of observed galaxies. If a large enough number of galaxies are observed, this effect can be separated from the intrinsic ellipticities of the galaxies which allows us to estimate the lensing potential.

To constrain cosmological parameters we can then look at the lensing potential of the CMB, $\psi_{\rm CMB}$, and of galaxy surveys, $\psi_{\rm gal}$. These are directly related to the matter power and bispectra as

$$C_\ell^{\psi_X\psi_Y} = \frac{9}{\ell^4}\Omega_m^2 H_0^4 \int_0^{\chi_*} \chi^2 \mathrm{d}\chi a(\eta_0-\chi)^{-2} W_X(\chi) W_Y(\chi) P^\delta(\ell/\chi, \eta_0-\chi), \tag{2.1}$$

$$\begin{aligned} B^{\psi_X\psi_Y\psi_Z}_{\ell\ell_1\ell\ell_2\ell\ell_3} &= \sqrt{\frac{(2\ell_1+1)(2\ell_2+1)(2\ell_3+1)}{4\pi}} \begin{pmatrix} \ell_1 & \ell_2 & \ell_3 \\ 0 & 0 & 0 \end{pmatrix} \frac{27}{\ell_1^2\ell_2^2\ell_3^2}\Omega_m^3 H_0^6 \\ &\times \int \chi^2 \mathrm{d}\chi a(\eta_0-\chi)^{-3} W_X(\chi) W_Y(\chi) W_Z(\chi) B^\delta(\{\ell_i/\chi\}, \eta_0-\chi), \end{aligned} \tag{2.2}$$

with $X, Y, Z \in \{\mathrm{CMB}, \mathrm{gal}\}$. A derivation can be found in appendices A and B, or in the literature; see, e.g. [6]. Ω_m is the present day matter density parameter. H_0 is the present-day Hubble constant, $a(\eta)$ is the scale factor, η_0 is the conformal time today and χ is the comoving radial distance. χ_* presents the distance to surface of last scattering. $P^\delta(k,\eta)$ is the matter power spectrum. $B^\delta(k_1,k_2,k_3,\eta)$ is the matter bispectrum. $W_X(\chi)$ is the window function. Finally,

$$\begin{pmatrix} \ell_1 & \ell_2 & \ell_3 \\ m_1 & m_2 & m_3 \end{pmatrix},$$

is the Wigner 3-j symbol. The difference between CMB and galaxy lensing is the window function, defined as

$$W_X(\chi) = \int_\chi^\infty \mathrm{d}\chi' p_X(\chi') \frac{\chi'-\chi}{\chi'\chi}, \tag{2.3}$$

with p_X the radial distribution of the radiation source. For the CMB we take $p(\chi) = \delta(\chi-\chi_*)$. The window function presents the distribution of redshifts at which a CMB photon or galaxy photon is deflected. As a result, the CMB lensing window function is broader and peaks at higher redshift compared to the galaxy window function.

Our convention for defining the linear and non-linear matter power spectrum is

$$\langle \delta(\mathbf{k},\eta)\delta(\mathbf{k}',\eta)\rangle = (2\pi)^3 \delta_D(\mathbf{k}+\mathbf{k}') P^\delta(\mathbf{k},\eta),$$

and for the bispectrum it is

$$\langle \delta(\mathbf{k}_1,\eta)\delta(\mathbf{k}_2,\eta)\delta(\mathbf{k}_3,\eta)\rangle = (2\pi)^3\delta_D(\mathbf{k}_1+\mathbf{k}_2+\mathbf{k}_3)B^\delta(k_1,k_2,k_3,\eta),$$

with δ the fractional matter density perturbation field and δ_D the Dirac delta function.

2.2 Nonlinear matter bispectrum

Determining the nonlinear matter power spectrum can be done using numerical codes such as CAMB [25]. The nonlinear matter bispectrum was calculated from the power spectrum using a fitting formula based on perturbation theory in [14]. It is given by

$$B^\delta(k_1,k_2,k_3,\chi) = 2F_2(k_1,k_2,z)P^\delta(k_1,z)P^\delta(k_2,z) + 2 \text{ perm}, \tag{2.4}$$

where P^δ is the nonlinear matter power spectrum[1], and the kernel F_2 is modified from the tree level result with factors $a(k,z)$, $b(k,z)$, and $c(k,z)$:

$$F_2(k_1,k_2,z) = \frac{5}{7}a(k_1,z)a(k_2,z) + \frac{k_1^2+k_2^2}{2k_1k_2}b(k_1,z)b(k_2,z)\cos\theta + \frac{2}{7}c(k_1,z)c(k_2,z)\cos^2\theta. \tag{2.5}$$

They are defined as:

$$a(k,z) = \frac{1+\sigma_8^{a_6}(z)\sqrt{0.7}Q(n_{\rm eff})(q^{a_1})^{n_{\rm eff}+a_2}}{1+(q^{a_1})^{n_{\rm eff}+a_2}}, \tag{2.6}$$

$$b(k,z) = \frac{1+0.2a_3(n_{\rm eff}+3)(q^{a_7})^{n_{\rm eff}+3+a_8}}{1+(q^{a_5})^{n_{\rm eff}+3.5+a_8}}, \tag{2.7}$$

$$c(k,z) = \frac{1+\left[\frac{4.5a_4}{1.5+(n_{\rm eff}+3)^4}\right](q^{a_5})^{n_{\rm eff}+3+a_9}}{1+(q^{a_5})^{n_{\rm eff}+3.5+a_9}}. \tag{2.8}$$

Here, $Q(n_{\rm eff})$ is given by:

$$Q(x) = \frac{4-2x}{1+2^{x+1}}. \tag{2.9}$$

The effective spectral index of the linear power spectrum is defined as:

$$n_{\rm eff} \equiv \frac{d\ln P_{\rm lin}^\delta(k)}{d\ln k}. \tag{2.10}$$

Additionally, q is given by:

$$q = \frac{k}{k_{\rm NL}}, \tag{2.11}$$

where $k_{\rm NL}$ is the scale at which nonlinearities become significant, satisfying:

$$4\pi k_{\rm NL}^3 P_{\rm lin}^\delta(k_{\rm NL},0) = 1. \tag{2.12}$$

The coefficients a_i are:

$$\begin{aligned} &a_1 = 0.484, \quad a_2 = 3.740, \quad a_3 = -0.849, \quad a_4 = 0.392, \\ &a_5 = 1.013, \quad a_6 = -0.575, \quad a_7 = 0.128, \quad a_8 = -0.722, \quad a_9 = -0.926. \end{aligned}$$

[1] Compare to the tree level bispectrum where we instead use the linear power spectrum.

2.3 Post-Born corrections

One of the approximations made in the derivation of the weak lensing power- and bispectra (equations (2.1) and (2.2)) is that the integral is performed along the line of sight to the light source. To get an analytically correct result, one would instead need to solve a differential equation with a feedback loop where the effects of gravitational lensing affect the trajectory and shape of given bundle of light rays which in turn changes the way future gravitational lenses affect the bundle. One can also choose to make order by order corrections to the Born approximation. There is motivation to understand the effects of these corrections (see the introduction) so we present them here.

Under the Born approximation, the elements of the distortion tensor, ψ_{ab}, (from which shear, convergence, and rotation are constructed) equal second derivatives of the lensing potential. We thus calculate the potential instead of the distortion tensor itself. When post-born effects are taken into account this is no longer true and we are forced to work with ψ_{ab} directly. Following [31], the leading order post born correction to the distortion tensor for a point source at distance χ_s is given by

$$\left(\psi_{ab}^{\text{p.s.}}\right)^{(2)}(\chi_s) := 2\int_0^\infty d\chi\,\chi^2\,\frac{\chi_s-\chi}{\chi_s\chi}\Theta(\chi_s-\chi)\left[-\Psi_{,ac}(\chi)\left(\psi_{cb}^{\text{p.s.}}\right)^{(1)}(\chi)+\Psi_{,acd}(\chi)\,\delta x_d^{(1)}(\chi)\right]. \tag{2.13}$$

Here $\left(\psi_{cb}^{(p.s.)}\right)^{(1)}(\chi)$ is the deformation for a point source at χ under the Born approximation as defined earlier. $\delta x_d^{(1)}(\chi)$ is the first order correction to the location of the lensed light ray at a distance χ, given by

$$\delta x_a^{(1)} = -2\int_0^\chi d\chi'\,\frac{\chi-\chi'}{\chi\chi'}\,\chi\chi'\,\Psi_{,a}(\chi'). \tag{2.14}$$

To adapt the above to a source with radial distribution $p(\chi)$ (which in our case will be a population of galaxies) we integrate over χ_s as follows:

$$(\psi_{ab}^{\text{gal}})^{(i)} = \int_0^\infty d\chi_s p(\chi_s)\left(\psi_{cb}^{(p.s.)}\right)^{(i)}(\chi_s). \tag{2.15}$$

This step essentially just changes $(\chi_s-\chi)/(\chi_s\chi)\Theta(\chi_s-\chi)$ in equation (2.13) to the window function $W(\chi)$ defined in equation (2.3).

The leading order correction to the convergence bispectrum of sources 1, 2, 3 is given as

$$B_{L_1L_2L_3}^{\kappa^{(1)}\kappa^{(2)}\kappa^{(3)}} = 2\frac{\mathbf{L}_1\cdot\mathbf{L}_2}{L_1^2L_2^2}\left[\mathbf{L}_1\cdot\mathbf{L}_3\mathcal{M}_s^{(1)(2)(3)}(L_1,L_2)+\mathbf{L}_2\cdot\mathbf{L}_3\mathcal{M}_s^{(2)(1)(3)}(L_2,L_1)\right]+\text{cyc. perm.}, \tag{2.16}$$

where

$$\mathcal{M}_s^{(1)(2)(3)}(L_1,L_2) := L_1^4\int_0^{\chi_s} d\chi\frac{W^{(1)}(\chi)W^{(3)}(\chi)}{\chi^2}P_{\Psi\Psi}\left(\frac{L_1}{\chi},z(\chi)\right)C_{L_2}^{\kappa^{(2)}\kappa^{(3)}}(\chi,\chi_s), \tag{2.17}$$

and

$$C_{L_2}^{\kappa^{(2)}\kappa^{(3)}}(\chi,\chi_s) := \int_0^\infty d\chi' W^{(2)}(\chi')\frac{\chi_s-\chi}{\chi_s\chi}\Theta(\chi_s-\chi)P_{\Psi\Psi}(\frac{L_2}{\chi'},\chi'). \tag{2.18}$$

2.4 Fisher matrix analysis

The signal-to-noise (SNR) and parameter constraints are obtained through a Fisher matrix analysis as is standard in cosmology[13]. A full derivation of the equations used below can be found in appendix C. The auto- and cross- power spectrum Fisher matrix is given as

$$F_{\alpha\beta} = \sum_{\ell} \sum_{XY} \sum_{X'Y'} (2\ell+1) \partial_\alpha C_\ell^{XY} (C^{-1})_\ell^{XX'} (C^{-1})_\ell^{YY'} \partial_\beta C_\ell^{X'Y'},$$

where

$$C_\ell := \begin{pmatrix} C_\ell^{\psi_{\rm CMB}\psi_{\rm CMB}} & C_\ell^{\psi_{\rm CMB}\psi_{\rm gal}} \\ C_\ell^{\psi_{\rm CMB}\psi_{\rm gal}} & C_\ell^{\psi_{\rm gal}\psi_{\rm gal}} \end{pmatrix}.$$

For the bispectra we instead have

$$F_{\alpha\beta} = \sum_{\ell_1 \le \ell_2 \le \ell_3} \frac{\mathcal{P}_{\ell_1\ell_2\ell_3}}{6} \sum_{XYZ} \sum_{X'Y'Z'} \partial_\alpha B_{\ell_1\ell_2\ell_3}^{XYZ} (C^{-1})_{\ell_1}^{XX'} (C^{-1})_{\ell_2}^{YY'} (C^{-1})_{\ell_3}^{ZZ'} \partial_\beta B_{\ell_1\ell_2\ell_3}^{X'Y'Z'},$$

with $\mathcal{P}_{\ell_1\ell_2\ell_3}$ defined as the number of distinct permutations that can be made with $\ell_1\ell_2\ell_3$. When only considering auto spectra the formulas simplify to:

$$F_{\alpha\beta} = \sum_{\ell} \sum_{XY} \sum_{X'Y'} \frac{2\ell+1}{2} \frac{\partial_\alpha C_\ell^{XX} \partial_\beta C_\ell^{XX}}{(C_\ell^{XX})^2},$$

and (for bispectra, assuming Gaussian, diagonal, covariance)

$$F_{\alpha\beta} = \sum_{\ell_1 \le \ell_2 \le \ell_3} \frac{\mathcal{P}_{\ell_1\ell_2\ell_3}}{6} \frac{\partial_\alpha B_{\ell_1\ell_2\ell_3}^{XXX} \partial_\beta B_{\ell_1\ell_2\ell_3}^{XXX}}{C_{\ell_1}^{XX} C_{\ell_2}^{XX} C_{\ell_3}^{XX}}.$$

If only some fraction of the sky, $f_{\rm sky}$, is measured, all Fisher matrices are multiplied by $f_{\rm sky}$ [35].

3 Experimental parameters and priors

3.1 Fiducial cosmology

Our fiducial cosmology is based on the Planck results [3] (see table 1). We choose to constrain the standard parameters of the ΛCDM model as well as neutrino mass, m_ν, and dark energy equation of state parameter, w_0. Our reason for including these extra degrees of freedom is that we would like to see to what degree future surveys will be able to tell us more about the mass of neutrinos and the nature of dark energy. For example, a paper from the DESI collaboration [32] recently showed that measurements of baryon acoustic oscillations give a 2.5 - 4 σ tension with a non-evolving dark energy equation of state model, so it is worth considering if future weak lensing experiments could tell us more about this tension. Regarding neutrinos, depending on how stage 4 surveys will be able to constrain neutrino mass, the results could tell us more about their mass hierarchy and serve as a test for constraints obtained from other probes, such as baryon acoustic oscillations.

3.2 Choice of priors

Throughout this paper we consider two priors. The first we refer to as our "weak prior" and is based on the one used in [30] (see table 1). This prior only restricts $\Omega_b h^2$ and n_s significantly, as those are not well constrained by lensing spectra alone. Our differences with [30] are that (i) we do not fix τ, but instead take it to have a SNR of 1 and added a loose A_s prior as well, (ii) instead of a flat prior for the Hubble constant ($40 < H_0 < 100$) we use a gaussian distribution with the same standard deviation, (iii) we added a weak constraint on $\Omega_c h^2$, and (iv) we also vary neutrino mass and w_0 but do not assume any constraints on them in our priors. The purpose of the weak prior is as follows. The weak lensing power spectra, in particular, exhibit complete insensitivity to certain parameters. Consequently, relying solely on them to constrain the entire cosmological model results in very poor constraints. Future lensing surveys will of course use information from surveys measuring other statistics such as those derived from galaxy clustering and the primary CMB anisotropies. By adding a prior based on these (primary) statistics our results become more representative. Additionally, by considering a conservative prior, it remains clear how the different lensing spectra complement each other. The other prior we consider is based on the CMB temperature and E-mode polarization cross- and auto-powerspectra from $\ell = 30$ to $\ell = 2000$ assuming the same noise properties as used for the CMB weak lensing reconstruction noise. Adopting these priors serve to test how weak lensing statistics are able to further tighten constraints beyond measuring primary statistics. It is worth noting that the constraint for τ and w_0 are tighter than in other literature (see [1] and [28] for comparable τ and w_0 constraints, respectively). Based on a number of internal tests[2] we suspect that this is mainly due us not taking into account foregrounds in our noise models.

parameter	**notation**	**fiducial value**	**σ of weak prior**	**σ of $T+E$ prior**
Hubble constant	H_0	67.4 km/s/Mpc	17.3	1.21
Physical baryon density parameter	$\Omega_b h^2$	0.0223	0.0005	0.000057
Physical cold dark matter density parameter	$\Omega_c h^2$	0.119	0.288	0.00083
Scalar spectral index	n_s	0.965	0.02	0.0025
Reionization depth	τ	0.063	0.063	0.0013
Amplitude of primordial scalar fluctuations	A_s	2.13×10^{-9}	1×10^{-9}	5.5×10^{-11}
Sum of neutrino masses	$\sum m_\nu$	0.06	∞	0.22
Dark energy equation of state parameter	w_0	-1	∞	0.058

Table 1. Cosmological parameters varied (ΛCDM + w_0 + m_ν). We use a prior similar to the one used by the Planck weak lensing results [30] which essentially only restricts $\Omega_b h^2$ and n_s significantly.

3.3 Noise Modeling

This paper considers noise levels for "stage 3" and "stage 4" (weak lensing) surveys. Noise properties considered for this analysis can be found in table 2, including experiments they are representative of. A comparison of the noise power spectra to the lensing power spectra are shown in figure 1. Effectively, for galaxy lensing, the power spectrum is signal-dominated up until $\ell \sim 200$ (stage 3) and $\ell \sim 700$ (stage 4). For CMB lensing, the power spectrum is signal-dominated for $\ell \sim 300$ (stage 3) and $\ell \sim 1000$ (stage 4).

The CMB lensing noise is estimated using a quadratic estimator [26]. The parameters characterizing the noise levels are beam width, σ, polarization white noise, Δ_P, and temperature white noise Δ_T.

[2]This included looking at the accuracy of numerical derivatives w.r.t. cosmological parameters, testing the numerical stability of Fisher matrices wr.r.t. matrix inversion, and varying our values for detector noise and beam width.

source	survey stage	noise vals	comparable experiments
CMB	stage 3	$\sigma = 1'$, $\Delta_P = 6'$ μK	Advanced ACTPol, Simons Observatory
	stage 4	$\sigma = 3'$, $\Delta_P = 1'$ μK	CMB-S4
galaxies	stage 3	$\sigma_{\rm rms} = 0.3$, $n_g = 5 {\rm arcmin}^{-2}$	DES, KiDS
	stage 4	$\sigma_{\rm rms} = 0.3$, $n_g = 30 {\rm arcmin}^{-2}$	LSST, Euclid

Table 2. Noise levels considered for weak lensing of galaxies and the CMB. σ (beam width) and Δ_P (polarization white noise) describe CMB survey specifications, while $\sigma_{\rm rms}$ (intrinsic galaxy ellipticity) and n_g (observed galaxy density) refer to galaxy shear surveys.

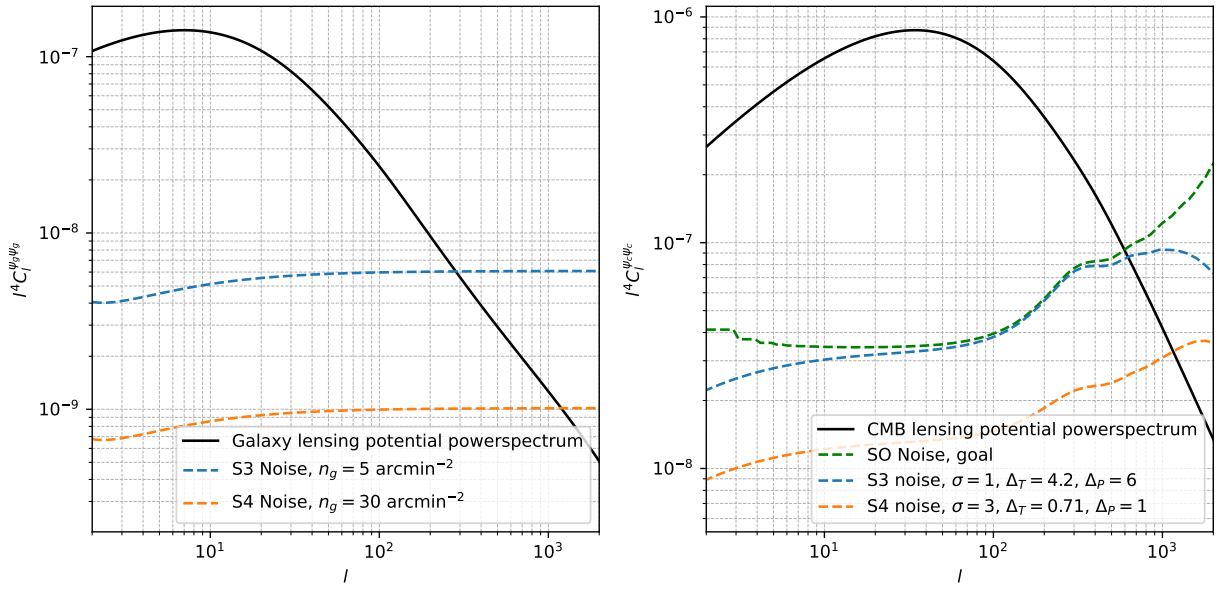

Figure 1. CMB (right) and galaxy (left) lensing potential power spectra compared to associated experimental noise. Current (stage 3) noise values are displayed as well as near future[4] (stage 4) noise values. The CMB lensing experiment uses only polarization. CMB noise values are chosen in accordance with [28]. For comparison we also how the reconstruction noise for the Simons Observatory. Shear noise values are chosen to be similar to e.g. Euclid measurements for stage 4 and e.g. KiDS for stage 3.

We take $\Delta_T = \Delta_P/\sqrt{2}$ throughout. Galaxy lensing is determined by measuring lensing shear (see appendices A and D). The noise in this measurement is dominated by scale-independent shot noise and has associated noise power spectrum $N_l^{\rm shear} = \sigma_{\rm rms}^2/n_g$, [6]. n_g is the amount of galaxies observed per unit solid angle. The noise power spectrum for the lensing potential then equals

$$N_\ell^{\text{lens. potential}} = \frac{4}{(\ell-1)\ell(\ell+1)(\ell+2)} N_\ell^{\rm shear}.$$

In all cases we assume that the proportion of the sky surveyed, $f_{\rm sky}$, equals 0.5. For parameter constraints, we will consider only stage 4 noise levels.

3.4 Other details

The redshift distribution of the observed galaxies is commonly parameterized as [6]

$$n(z) \propto z^a \exp\left[-\left(\frac{z}{z_0}\right)^b\right].$$

We choose the parameter combination $a = 2$, $b = 3/2$ and $z_0 = 0.64$ which is similar to the expected distributions of Euclid, (which will probe primarily in the 0.2 - 2.6 redshift range [12]) and the LSST mission (which has $a \approx 2$, $b \approx 1$, and $z_0 \approx 0.3$ from predictions for the obtained data [19]). For simplicity, we do not implement a tomographic binning of the source galaxies, and instead model the population with a single effective redshift distribution.

Derivatives are calculated with a central difference formula (see appendix E for convergence). To check the accuracy of our results we calculated constraints for similar experimental parameters as in references [30, 35, 1, 29] and found good agreement in all cases.

4 Results

4.1 Detectability

As expected, lensing power spectra should be detectable at high signal-to-noise. The signal-to-noise of the CMB and galaxy lensing bispectra versus the maximum multipole moment measured is shown in figure 2. In the absence of systematics, shear bispectra can be detected at high signal-to-noise with both stage 3 and stage 4 experiments. CMB lensing bispectra could be detectable by a stage 3 experiment (see e.g. ref. [22] for the effect of noise biases) and with high signal-to-noise with a stage 4 experiment. Our results for CMB weak lensing S/N match those of reference [28].

Regarding post-Born corrections, we found that the effect on the galaxy lensing bispectrum S/N is a few percent at most, in agreement with [7]. We thus did not include additional plots for these corrections. For the CMB the S/N is reduced significantly (in agreement with [31]) but not so severely that they are no longer detectable. Our conclusions thus remain the same: the CMB bispectrum is probably detectable with stage 3 surveys and definitely detectable with stage 4 surveys.

4.2 Parameter Constraints

Next, we consider cosmological parameter constraints. We include both the power spectrum and the bispectrum of the weak lensing. We look at two extension of ΛCDM, m_ν and w_0 as well as the derived parameters σ_8, and Ω_m. Constraints on the full set of ΛCDM parameters can be found in appendix F. Results shown include marginalization over all parameters. Figures 3 and 5 show confidence ellipses from stage 4 CMB and galaxy lensing surveys assuming a weak prior, respectively. Figures 4 and 6 show confidence ellipses in the case of our primary CMB $T + E$ prior. Table 3 summerizes all forecasted constraints.

Constraints are significantly improved by including bispectrum information in nearly all cases when using weak priors. When including the CMB $T + E$ priors, both the CMB lensing power-

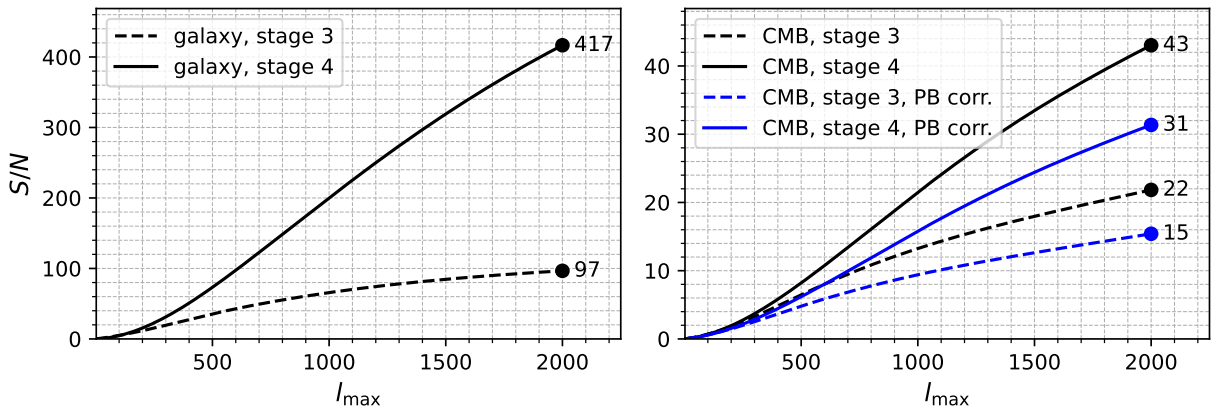

Figure 2. Signal-to-noise ratios for galaxy lensing (left) and CMB lensing (right) bispectra for stage 3 (dashed) and stage 4 (not dashed) surveys as a function of maximum multipole measured. The minimum multipole is always $l_{\rm min} = 2$. The multipole range used for CMB lensing reconstruction is $2 \leq \ell \leq 10^4$. Using a more conservative range such as $30 \leq \ell \leq 5000$ used to calculate Simons Observatory noise curves don't significantly affect the results.

and bispectra significantly improve prior constraints, however combining them does not lead to significant improvements compared to only using lensing power spectra. For galaxy lensing, the power- and bispectra yield nearly identical improvements compared to the CMB $T + E$ prior. In this case, combining both statistics leads to significantly tighter constraints (in contrast to CMB lensing). When combining CMB and galaxy lensing we see that the bispectrum is slightly less competitive compared to the lensing power spectrum, but can still significantly improve constraints compared to only using the lensing power spectrum.

Furthermore, it is clear that, in general, combining CMB and galaxy lensing surveys also leads to significant improvements in constraining power, even in the case of a strong CMB $T+E$ prior. The improvement is most significant for the neutrino mass constraint.

Besides these obvious findings, we make several other conclusions:

- Lensing power spectra alone are not sufficient to competitively constrain $\Lambda\text{CDM} + w_0 + m_\nu$ without priors, even in the case of stage 4 surveys.
- For lower noise values (in particular for stage 4 noise) the bispectra become increasingly important compared to the powerspectra. The lensing bispectra are directly related to the amount of non-gaussianity in the matter distribution. As noise levels become lower, we are able to measure the matter distribution on small enough scales where nonlinear matter evolution becomes important. Additionally, for galaxy lensing, the window function peaks at later redshifts than compared to CMB lensing. The bispectrum is largest at late times, and thus the galaxy lensing bispectrum is significantly easier to detect and is better at constraining parameters then the CMB lensing bispectrum.
- The information from bispectra is sensitive to cosmology in a different way than that of the power spectra. The main parameter combinations where approximate degeneracies are

weak priors (with and without post-Born corrections)										
		CMB lensing			Gal. lensing			CMB × Gal. lensing		
Par	prior	C_ℓ	$B_{\ell_1\ell_2\ell_3}$	$C_\ell + B_{\ell_1\ell_2\ell_3}$	C_ℓ	$B_{\ell_1\ell_2\ell_3}$	$C_\ell + B_{\ell_1\ell_2\ell_3}$	C_ℓ	$B_{\ell_1\ell_2\ell_3}$	$C_\ell + B_{\ell_1\ell_2\ell_3}$
m_ν	10	0.28	1.1	0.23	1.0	0.26	0.16	0.10	0.13	0.065
			1.2	0.18		0.33	0.21		0.18	0.063
w_0	10	0.54	1.4	0.37	0.26	0.078	0.025	0.059	0.066	0.019
			0.82	0.31		0.083	0.028		0.063	0.020
σ_8	2.5	0.12	0.19	0.055	0.081	0.037	0.013	0.014	0.016	0.0080
			0.18	0.057		0.040	0.013		0.018	0.0084
Ω_m	0.67	0.19	0.18	0.073	0.14	0.048	0.017	0.016	0.016	0.0072
			0.18	0.071		0.055	0.018		0.018	0.0073
CMB $T + E$ priors (with and without post-Born corrections)										
		CMB lensing			Gal. lensing			CMB × Gal. lensing		
Par	prior	C_ℓ	$B_{\ell_1\ell_2\ell_3}$	$C_\ell + B_{\ell_1\ell_2\ell_3}$	C_ℓ	$B_{\ell_1\ell_2\ell_3}$	$C_\ell + B_{\ell_1\ell_2\ell_3}$	C_ℓ	$B_{\ell_1\ell_2\ell_3}$	$C_\ell + B_{\ell_1\ell_2\ell_3}$
m_ν	0.22	0.074	0.12	0.073	0.14	0.10	0.086	0.043	0.090	0.037
			0.13	0.073		0.12	0.099		0.10	0.038
w_0	0.058	0.046	0.053	0.046	0.048	0.039	0.021	0.032	0.037	0.017
			0.053	0.046		0.042	0.022		0.039	0.018
σ_8	0.015	0.014	0.015	0.013	0.013	0.011	0.0079	0.0097	0.010	0.0061
			0.015	0.014		0.012	0.0077		0.011	0.0063
Ω_m	0.015	0.014	0.015	0.014	0.013	0.011	0.0087	0.010	0.0096	0.0055
			0.015	0.014		0.011	0.0085		0.010	0.0057

Table 3. Parameter constraints for different combinations of weak lensing information. C stands for powerspectra, and B for bispectra. All surveys are assumed to be stage 4 surveys with multipole range $2 \leq \ell \leq 2000$. We use the weak and CMB priors described in table 1. The blue colored rows show constraints from bispectra with post-Born corrections. Post-Born corrections are not taken into account for the lensing powerspectra as mentioned earlier, so these values are ommited in the blue rows.

broken are $(n_s, \Omega_b h^2)$, $(\Omega_b h^2, H_0)$, $(\Omega_c h^2, H_0)$, $(\Omega_c h^2, \Omega_b h^2)$ $(n_s, \Omega_c h^2)$, (m_ν, H_0), (m_ν, n_s), $(A_s, \Omega_b h^2)$ (see also appendix F). This means that even if stage 4 surveys are not able to reach the noise levels assumed in this paper, the bispectra will likely still lead to significantly tighter constraints.

- Stage 4 galaxy weak lensing surveys generally contain more information than CMB surveys. Comparing the confidence ellipses, it is clear that the two types of surveys depend on the underlying parameters in different ways. This leads to substantially better constraints for σ_8, Ω_m, m_ν, and w_0 when combining CMB and galaxy lensing.

- It is clear that post-Born corrections do not change the constraints drastically. As expected, they matter less for galaxy lensing and when using the CMB $T + E$ prior. Interestingly, although the constraints due to bispectra alone are always worse, for some parameters they are instead improved when combining lensing bispectrum information with that of the lensing powerspectrum. This implies that, at least in some cases, the post-Born contribution to the lensing bispectrum depends on the parameters in a different way than the lensing powerspectrum and thus improves the amount of information we can extract from survey data despite making the lensing bispectrum less detectable. Besides these observations, we conclude that taking into account post-Born corrections does not lead to different conclusions about the overall sensitivity of the lensing spectra.

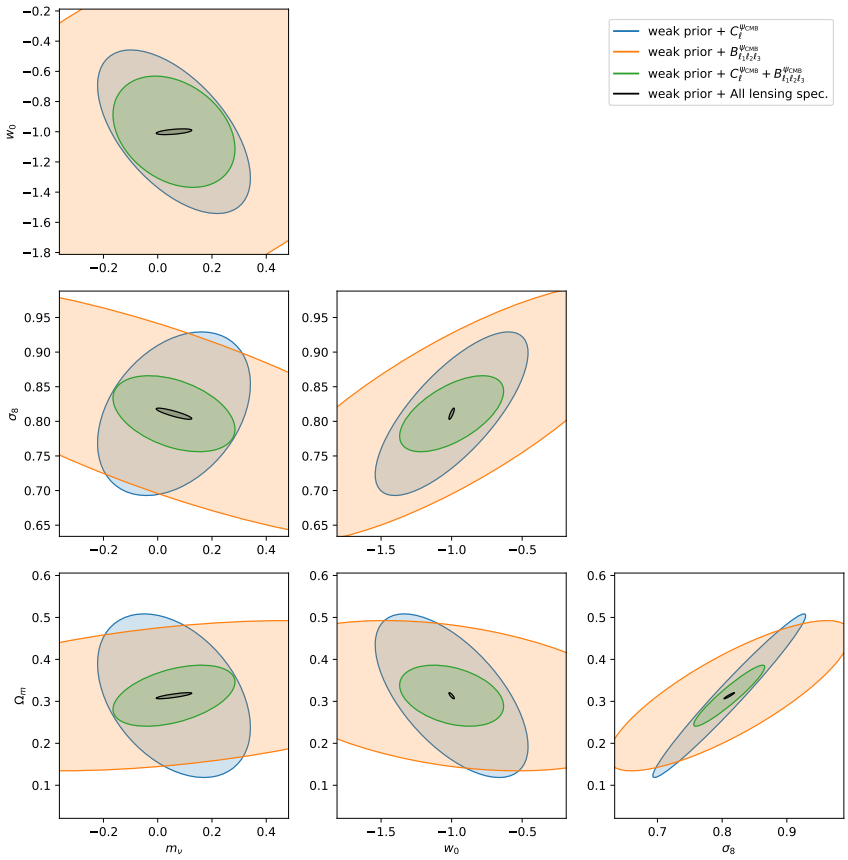

Figure 3. Parameter constraints and confidence ellipses for μ_ν, w_0, σ_8, and Ω_m. Using "stage 4" noise with multipole range from 2 to 2000. The colored plots show CMB lensing power- and/or bispectrum constraints. We use the weak priors listed in table 1. The confidence ellipses are for 1σ certainty. They show approximate degeneracies in the information gained from a survey if they are "stretched". When the information of ellipses with degeneracies in different directions is combined, the degeneracies are removed and the constraints typically becomes much better on the relevant parameters. The black plots show the constraints using all lensing information, i.e. CMB lensing spectra, galaxy lensing spectram, and all cross spectra.

5 Discussion and conclusion

In this work, we have presented parameter forecasts from CMB lensing and galaxy lensing power- and bispectra, considering experimental parameters representative of Stage 3 and Stage 4 CMB and galaxy surveys. Our analysis shows that while lensing power spectra are detectable at high significance, the inclusion of bispectra generally offers significant improvements when considering parameter constraints when considering an LCDM+ model of the universe. Notably, both CMB and galaxy bispectra are found to be detectable, even with Stage 3 experimental noise levels.

The primary impact of incorporating bispectrum information is a tightening of cosmological parameter constraints, particularly for parameters such as H_0, σ_8, and Ω_m, and in breaking key parameter degeneracies. We found that for sufficiently low noise levels, characteristic of Stage 4 surveys, the bispectra themselves can offer constraining power comparable to that of the power spectra, due to nonlinear structure formation on small scales being better detected by these future surveys. Fur-

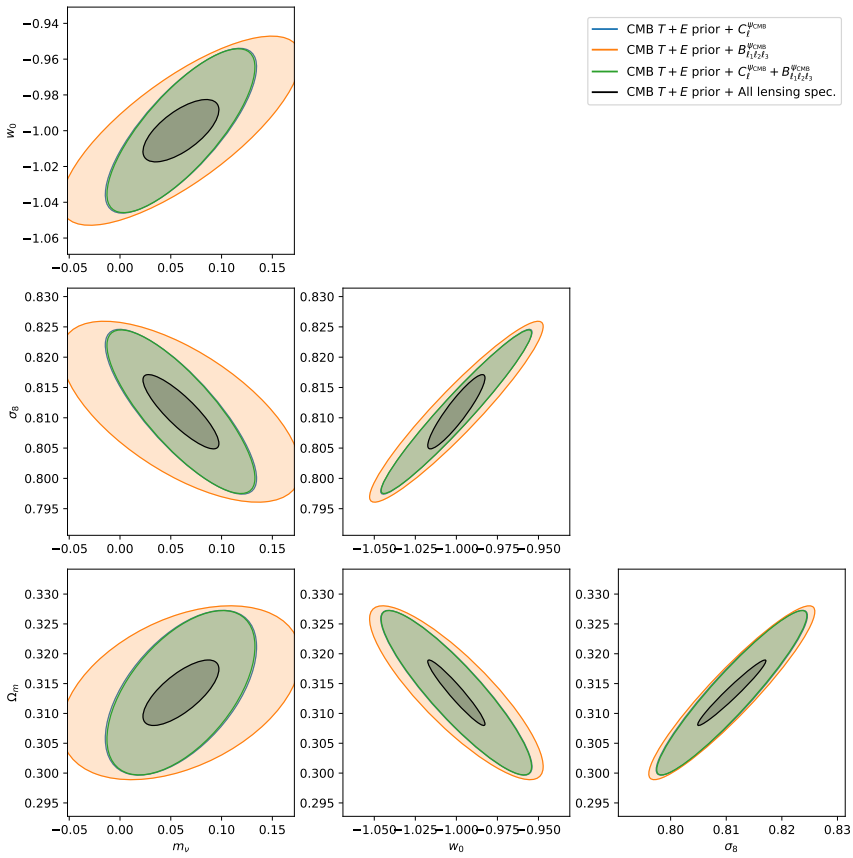

Figure 4. Same as figure 3, except we use the CMB temperature and polarization based priors listed in table 1.

thermore, the combination of CMB and galaxy lensing probes, especially when both power spectra and bispectra are utilized, further enhances constraints and aids in mitigating degeneracies. If all information were to be combined[5] we find particularly tight constraints on neutrino mass and dark energy equation of state in particular, i.e. $\sigma(m_\nu) = 55$ meV and $\sigma(w_0) = 0.017$. However, lensing power spectra alone, even for Stage 4 surveys, appear insufficient to competitively constrain an 8-parameter $\Lambda\text{CDM} + w_0 + \sum m_\nu$ model without any priors.

There are a number of limitations to the results presented in this paper. The limitations inherent to the Fisher matrix formalism and to non-physical noise models such as those considered in this paper are already well known. The main limitations specific to this work are:

- The fitting formula used for the nonlinear matter bispectrum (from [14]) has an estimated accuracy of only up to about 10 percent. This intrinsic inaccuracy in the model for B^δ will propagate to the lensing bispectra.
- Certain cosmological parameters that affect nonlinear large-scale structure, such as neutrino masses, likely alter the fitting parameters of the matter bispectrum formula when varied. In the literature, this is currently not considered, which can make the derivatives of the bispectrum with respect to these cosmological parameters less accurate.

[5] And using the CMB $T + E$ prior.

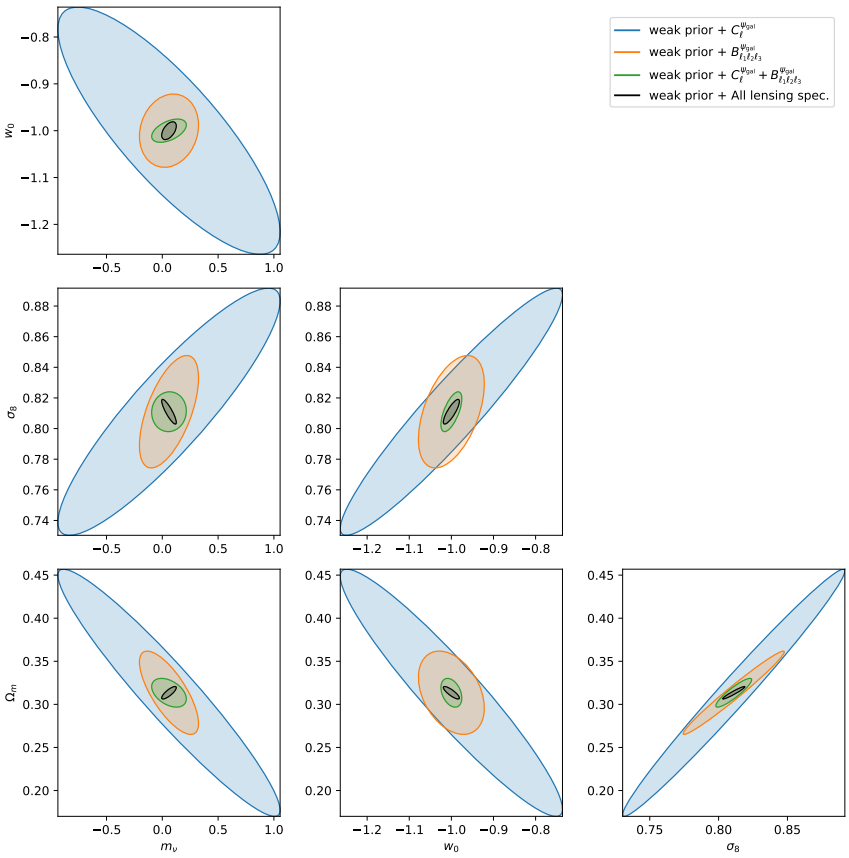

Figure 5. Same as figure 3, except here the colored plots show galaxy lensing constraints.

- We assumed throughout this paper that surveys would measure multipoles as low as $\ell = 2$. However, our analytical formulas to calculate lensing spectra utilize the Limber approximation, which is only robust for $\ell \gtrsim 50$. Avoiding the Limber approximation would complicate calculations, requiring knowledge of unequal-time matter power and bispectra, and would be computationally much more demanding due to the need to evaluate double integrals instead of single integrals. With the methods used in this paper, recalculating Fisher matrices without the Limber approximation would not be feasible, even if unequal-time matter spectra were readily available. Methods such as those explored in reference [10] might offer a path to address this.

- As noted in appendix C, the Gaussian approximation was used for the covariance of the spectra estimators, i.e. we ignored any contributions not arising from standard Wick contractions. We know that the estimated lensing potential is not Gaussian in general, for two reasons: (i) The matter distribution is not Gaussian. (ii) Even with a Gaussian matter distribution, the quadratic estimator we used will not be Gaussian. Consider, for example, $\langle\hat{\phi}\hat{\phi}\hat{\phi}\hat{\phi}\rangle$. Each $\hat{\phi}$ is given as a sum over products of the lensing CMB anisotropies, T, E, B. Writing out each $\hat{\phi}$ in this way would yield terms such as $\langle TTTTTT\rangle$ (i.e. 6 point functions). These terms are non-zero. In fact, not only would they give products of 2 point functions due to Wick contractions, but also connected n-point functions with $n > 2$ because the lensed fields are no longer Gaussian even if the original fields are. A next step could thus be to account for these

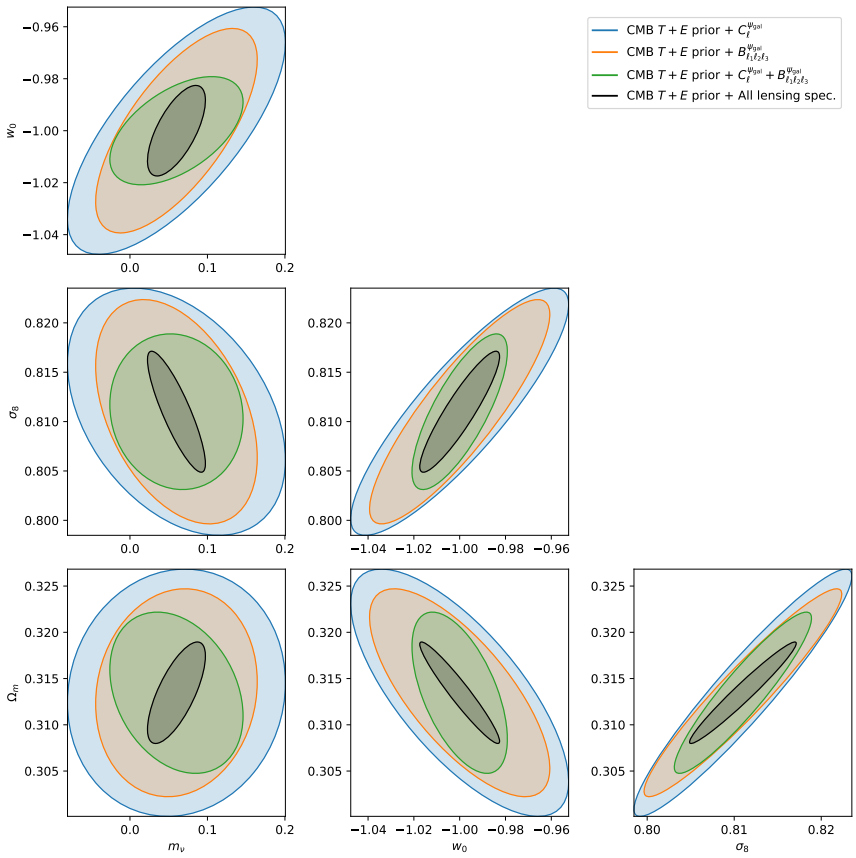

Figure 6. Same as figure 4, except here the colored plots show galaxy lensing constraints.

additional contributions, perhaps through N-body and ray-tracing simulations. Notably, such simulations could potentially also allow for a more accurate calculation of the lensing spectra themselves, without relying on fitting formulas for the matter bispectrum or the Limber approximation, depending on simulation accuracy.

- Related to the previous point, for a completely correct analysis we would also need to take into account correlations between a CMB prior and the lensing power- and bispectra. Currently we simply add Fisher matrices, however taking these correlations into account means computing a covariance matrix for combinations of T, E, ϕ with nonzero entries for correlations between T/E and ϕ. For instance, consider the correlation between the estimator of the temperature powerspectrum and the lensing powerspectrum at arbitrary multipoles. We will get terms like $\langle TT\hat{\phi}\hat{\phi}\rangle$, which will be a sum over 6 point functions like $\langle TTTETE\rangle$ due to our quadratic estimator. These 6 point functions are clearly non-zero, as explained earlier.

- The CMB lensing noise was estimated via a quadratic estimator. While standard, such estimators may not be strictly optimal, especially with complex foregrounds or non-Gaussianities. Estimators that, given our Stage 4 noise parameters, perform better do exist; for example, the iterative estimator developed in [34] can lead to a significantly better signal-to-noise ratio for the CMB lensing bispectrum, as shown in [28]. Using such an iterative estimator may also result in the CMB bispectrum being able to significantly improve parameter constraints when combined with lensing power spectra and a CMB $T+E$ prior.

- To calculate the Fisher matrices, derivatives of the lensing spectra with respect to cosmological parameters were computed using a central difference formula. This introduces errors (estimated at most a few percent, though larger for neutrino mass derivatives, see appendix E). Functions such as the matter power spectrum and fitting parameters for the matter bispectrum were approximated using pre-generated data and interpolation, also introducing errors of at most a few percent. Currently, these numerical errors are not considered significant because this paper primarily aims to provide a qualitative understanding of the utility of CMB and galaxy weak lensing spectra. However, for precise quantitative results, these factors would need to be revisited and improved.

- A 2024 paper [31] has shown that the Born approximation used to derive the formulas for the lensing power and bispectra, is no longer negligible for the lensing bispectrum. The post-Born corrections calculated in that paper only changed the lensing power spectra by $\leq 0.2\%$, while for the bispectra this effect was much larger, in particular for folded configurations. For future work it would thus be worthwile to analyze how these post-Born corrections affect the results presented in this paper.

- We did not model foreground contamination such as the cosmic infrared background (CIB), thermal Sunyaev-Zel'dovich (tSZ) effect, or point sources. These foregrounds can bias lensing reconstructions and bispectra, particularly in CMB–galaxy cross-correlations, and should be accounted for in future analyses.

Despite these limitations, this work provides valuable insight into the potential of future weak lensing surveys. Addressing these limitations will be crucial for obtaining robust cosmological constraints from upcoming observational data.

Acknowledgements

We would like to thank Prof. Toshiya Namikawa for providing extra details on his paper on the CMB lensing bispectrum [28], which, in particular, allowed us to cross check (intermediate) results. We would also like to thank Prof. Antony Lewis for looking at and confirming the correctness of the formulas for post-Born corrections in the case of a source with some redshift distribution. Finally, the authors thank Luna Jansma, who wrote a MSc thesis on the same subject, which served as the foundation of this study.

References

[1] Kevork N. Abazajian et al. *CMB-S4 Science Book, First Edition*. 2016. arXiv: 1610.02743 [astro-ph.CO]. URL: https://arxiv.org/abs/1610.02743.

[2] PAR Ade, J Aguirre, Z Ahmed, et al. "The Simons Observatory: science goals and forecasts". In: *Journal of Cosmology and Astroparticle Physics* 2019.02 (2019), p. 056.

[3] N. Aghanim et al. "Planck2018 results: VI. Cosmological parameters". In: *Astronomy and Astrophysics* 641 (Sept. 2020), A6. ISSN: 1432-0746. DOI: 10.1051/0004-6361/201833910. URL: http://dx.doi.org/10.1051/0004-6361/201833910.

[4] D. Bacon, A. Refregier, and R. Ellis. "Detection of weak gravitational lensing by large-scale structure". In: *Monthly Notices of the Royal Astronomical Society* 318 (2000), pp. 625–640.

[5] Matthias Bartelmann and Peter Schneider. "Weak gravitational lensing". In: *Physics Reports* 340 (2001), pp. 291–472.

[6] Matthias Bartelmann and Peter Schneider. "Weak Gravitational Lensing". In: *Physics Reports* 340.4-5 (2001), pp. 291–472. DOI: 10.1016/S0370-1573(00)00082-X.

[7] Alexandre Barthelemy, Sandrine Codis, and Francis Bernardeau. "Post-Born corrections to the one-point statistics of (CMB) lensing convergence obtained via large deviation theory". In: *Monthly Notices of the Royal Astronomical Society* 494.3 (Apr. 2020), 3368–3382. ISSN: 1365-2966. DOI: 10.1093/mnras/staa931. URL: http://dx.doi.org/10.1093/mnras/staa931.

[8] F. Bernardeau, L. Van Waerbeke, and Y. Mellier. "Weak lensing statistics as a probe of non-Gaussian initial conditions". In: *Astronomy & Astrophysics* 322 (1997), pp. 1–18.

[9] George Casella and Roger L. Berger. *Statistical Inference*. 2nd. Duxbury Pacific Grove, CA, 2002. ISBN: 9780534243128.

[10] Shu-Fan Chen, Hayden Lee, and Cora Dvorkin. "Precise and accurate cosmology with CMB×LSS power spectra and bispectra". In: *JCAP* 05 (2021), p. 030. DOI: 10.1088/1475-7516/2021/05/030. arXiv: 2103.01229 [astro-ph.CO].

[11] Asantha Cooray and Wayne Hu. "Weak Gravitational Lensing Bispectrum". In: *The Astrophysical Journal* 548.1 (Feb. 2001), pp. 7–18. ISSN: 1538-4357. DOI: 10.1086/318660. URL: http://dx.doi.org/10.1086/318660.

[12] Euclid Collaboration: G. Desprez, S. Paltani, J. Coupon, et al. "Euclid Preparation - X. The Euclid Photometric-Redshift Challenge". In: *Astronomy and Astrophysics* 644 (2020), A31. DOI: 10.1051/0004-6361/202039403. URL: https://www.aanda.org/articles/aa/pdf/2020/12/aa39403-20.pdf.

[13] Scott Dodelson and Fabian Schmidt. *Modern Cosmology*. 2nd. Elsevier, 2020. ISBN: 978-0-12-815948-4.

[14] Hector Gil-Marin et al. "An improved fitting formula for the dark matter bispectrum". In: *Journal of Cosmology and Astroparticle Physics* 2012.02 (2012), p. 047. DOI: 10.1088/1475-7516/2012/02/047. arXiv: 1111.4477 [astro-ph.CO].

[15] Christopher M. Hirata and Uroš Seljak. "Reconstruction of lensing from the cosmic microwave background polarization". In: *Physical Review D* 68.8 (Oct. 2003). ISSN: 1089-4918. DOI: 10.1103/physrevd.68.083002. URL: http://dx.doi.org/10.1103/PhysRevD.68.083002.

[16] Henk Hoekstra and Bhuvnesh Jain. "Weak Gravitational Lensing and Its Cosmological Applications". In: *Annual Review of Nuclear and Particle Science* 58.1 (2008), pp. 99–123.

[17] Wayne Hu and Takemi Okamoto. "Mass Reconstruction with Cosmic Microwave Background Polarization". In: *The Astrophysical Journal* 574.2 (Aug. 2002), pp. 566–574. ISSN: 1538-4357. DOI: 10.1086/341110. URL: http://dx.doi.org/10.1086/341110.

[18] Ž. Ivezić, S. M. Kahn, J. A. Tyson, et al. "LSST: From Science Drivers to Reference Design and Anticipated Data Products". In: *The Astrophysical Journal* 873.2 (2019), p. 111.

[19] Steven M. Kahn, Justin R. Bankert, Srinivasan Chandrasekharan, et al. "LSST System Performance". In: *LSST Science Book, Version 2.0*. Accessed: 2025-02-11. 2009. URL: https://www.lsst.org/sites/default/files/docs/sciencebook/SB_3.pdf.

[20] N. Kaiser, G. Wilson, and G. Luppino. "Large-Scale Cosmic Shear Measurements". In: *arXiv preprint astro-ph/0003338* (2000).

[21] Alba Kalaja, P. Daniel Meerburg, and William R. Pimentel Guilherme L.and Coulton. "Fundamental limits on constraining primordial non-Gaussianity". In: *Journal of Cosmology and Astroparticle Physics* 2021.04 (Apr. 2021), p. 050. ISSN: 1475-7516. DOI: 10.1088/1475-7516/2021/04/050. URL: http://dx.doi.org/10.1088/1475-7516/2021/04/050.

[22] Alba Kalaja et al. "The reconstructed CMB lensing bispectrum". In: *Journal of Cosmology and Astroparticle Physics* 2023.04 (Apr. 2023), p. 041. ISSN: 1475-7516. DOI: 10.1088/1475-7516/2023/04/041. URL: http://dx.doi.org/10.1088/1475-7516/2023/04/041.

[23] Martin Kilbinger. "Cosmology with cosmic shear observations: a review". In: *Reports on Progress in Physics* 78.8 (2015), p. 086901. DOI: 10.1088/0034-4885/78/8/086901. URL: https://arxiv.org/abs/1411.0115.

[24] R. Laureijs and others (Euclid Collaboration). *Euclid Definition Study Report*. ESA/SRE(2011)12. 2011. arXiv: 1110.3193.

[25] Antony Lewis, Anthony Challinor, and Anthony Lasenby. "Efficient computation of cosmic microwave background anisotropies in closed FRW models". In: *The Astrophysical Journal* 538 (2000), pp. 473–476.

[26] Abhishek S Maniyar et al. "Quadratic Estimators for CMB Weak Lensing". In: *arXiv preprint arXiv:2101.12193* (2021).

[27] Abhishek S. Maniyar et al. "Quadratic estimators for CMB weak lensing". In: *Phys. Rev. D* 103.8 (2021), p. 083524. DOI: 10.1103/PhysRevD.103.083524. arXiv: 2101.12193 [astro-ph.CO].

[28] Toshiya Namikawa. "CMB lensing bispectrum from nonlinear growth of the large scale structure". In: *Physical Review D* 93.12 (June 2016). ISSN: 2470-0029. DOI: 10.1103/physrevd.93.121301. URL: http://dx.doi.org/10.1103/PhysRevD.93.121301.

[29] Z. Pan and L. Knox. "Constraints on neutrino mass from cosmic microwave background and large-scale structure". In: *Monthly Notices of the Royal Astronomical Society* 454.3 (Oct. 2015), 3200–3206. ISSN: 1365-2966. DOI: 10.1093/mnras/stv2164. URL: http://dx.doi.org/10.1093/mnras/stv2164.

[30] Planck Collaboration. "Planck 2018 results. VIII. Gravitational lensing". In: *arXiv e-prints* (July 2018). arXiv: 1807.06210 [astro-ph.CO].

[31] Geraint Pratten and Antony Lewis. "Impact of post-Born lensing on the CMB". In: *Journal of Cosmology and Astroparticle Physics* 2016.08 (Aug. 2016), 047–047. ISSN: 1475-7516. DOI: 10.1088/1475-7516/2016/08/047. URL: http://dx.doi.org/10.1088/1475-7516/2016/08/047.

[32] Nandan Roy et al. "Dynamical dark energy in the light of DESI 2024 data". In: *arXiv preprint* (2024). arXiv: 2406.00634 [astro-ph.CO]. URL: https://arxiv.org/abs/2406.00634.

[33] Charles Shapiro and Asantha Cooray. "The Born and lens–lens corrections to weak gravitational lensing angular power spectra". In: *Journal of Cosmology and Astroparticle Physics* 2006.03 (Mar. 2006), 007–007. ISSN: 1475-7516. DOI: 10.1088/1475-7516/2006/03/007. URL: http://dx.doi.org/10.1088/1475-7516/2006/03/007.

[34] Kendrick M Smith et al. "Delensing CMB polarization with external datasets". In: *Journal of Cosmology and Astroparticle Physics* 2012.06 (June 2012), pp. 014–014. ISSN: 1475-7516. DOI: 10.1088/1475-7516/2012/06/014. URL: http://dx.doi.org/10.1088/1475-7516/2012/06/014.

[35] M. Takada and B. Jain. "Cosmological parameters from lensing power spectrum and bispectrum tomography". In: *Monthly Notices of the Royal Astronomical Society* 340 (2003), pp. 580–608.

[36] Max Tegmark. "Cosmic Confusion: Degeneracies among Cosmological Parameters Derived from Measurements of Microwave Background Anisotropies". In: *Monthly Notices of the Royal Astronomical Society* 294.2 (1997), pp. 337–348. DOI: 10.1093/mnras/294.2.337.

[37] L. Van Waerbeke, Y. Mellier, T. Erben, et al. "Detection of correlated galaxy ellipticities from CFH12k VLT data: first evidence for gravitational lensing by large-scale structures". In: *Astronomy & Astrophysics* 358 (2000), pp. 30–44.

[38] L. van Waerbeke et al. "Measurement of cosmic shear three-point correlations in the VIRMOS-Descart survey". In: *Astronomy and Astrophysics* 393 (2002), pp. 369–381. arXiv: astro-ph/0101511 [astro-ph].

A Weak Lensing

A.1 Perturbed Photon Paths

We work in the conformal Newtonian gauge and with natural units. Denoting conformal time and conformal radial distance by η and χ, respectively, the perturbed line element in FLRW spacetime is given by

$$\mathrm{d}s^2 = a^2(\eta)((1+2\Psi_N)\mathrm{d}\eta^2 - (1+2\Phi_N)\gamma_{ij}\mathrm{d}x^i\mathrm{d}x^j), \tag{A.1}$$

where γ_{ij} is the unperturbed line element

$$\gamma_{ij} = \mathrm{d}x^i\mathrm{d}x^j = \mathrm{d}\chi^2 + f_K^2(\chi)(\mathrm{d}\theta^2 + \sin^2\theta\mathrm{d}\phi^2), \tag{A.2}$$

and $f_K(\chi)$ is the comoving angular diameter distance. We will hereafter only consider a flat universe so that $f_K(\chi) = \chi$. Weak lensing of a point source can be quantified by looking at the deflection field $\mathbf{d}(\hat{\mathbf{n}}) = \theta_{\mathrm{obs}} - \theta_{\mathrm{true}}$, i.e. the (small) difference between the angle at which we see the object and the angle at which we would see the object had no lensing occurred. To first order in Ψ_N and Φ_N, the deflection is given as [13]

$$\mathbf{d}(\hat{\mathbf{n}}) = -2\int_0^{\chi_*}\mathrm{d}\chi\frac{\chi_*-\chi}{\chi_*\chi}\nabla_{\hat{\mathbf{n}}}\Psi(\chi\hat{\mathbf{n}};\eta_0-\chi), \tag{A.3}$$

where Ψ is the Weyl Potential, $\Psi := (\Psi_N - \Phi_N)/2$, and χ_* is the conformal distance to the source. $\nabla_{\hat{\mathbf{n}}}$ is the derivative along the axes orthogonal to the line of sight. The above equation can be written in terms of the lensing potential, ψ, as $\mathbf{d}(\hat{\mathbf{n}}) = \nabla_{\hat{\mathbf{n}}}\psi(\hat{\mathbf{n}})$, with

$$\psi(\hat{\mathbf{n}}) := -2\int_0^{\chi_*}\mathrm{d}\chi\frac{\chi_*-\chi}{\chi_*\chi}\Psi(\chi\hat{\mathbf{n}};\eta_0-\chi). \tag{A.4}$$

If the source is instead distributed over radial distance according to some distribution function $p(\chi)$, with $p(\chi)$ normalized to integrate to 1, the $(\chi_* - \chi)/(\chi_*\chi)$ factor is changed as

$$\frac{\chi_* - \chi}{\chi_*\chi} \to W(\chi) := \int_\chi^\infty \mathrm{d}\chi' p(\chi') \frac{\chi' - \chi}{\chi'\chi}.$$

$W(\chi)$ is then called the window function. In the most general case, the lensing potential is thus given by

$$\psi(\hat{\mathbf{n}}) := -2 \int_0^\infty \mathrm{d}\chi W(\chi) \Psi(\chi\hat{\mathbf{n}}; \eta_0 - \chi). \tag{A.5}$$

The integration limit is sometimes also taken to be the surface of the last scattering, as any window function vanishes after that distance. In the case of CMB lensing we can take $p(\chi') = \delta(\chi' - \chi_*)$, in which case the window function reduces to $H(\chi_* - \chi)(\chi_* - \chi)/(\chi_*\chi)$, with $H(\chi)$ the Heaviside step function.

A.2 Convergence and Shear

The magnification matrix is defined as

$$A_{ij} := \delta_{ij} + \frac{\partial}{\partial n_j} d_i(\hat{\mathbf{n}}). \tag{A.6}$$

This matrix can be decomposed in the following form, which immediately gives us definitions for the **convergence**, κ, **shear**, γ_1 and γ_2, and **rotation**, ω:

$$A_{ij}(\hat{\mathbf{n}}) = \begin{pmatrix} 1 - \kappa - \gamma_1 & -\gamma_2 + \omega \\ -\gamma_2 - \omega & 1 - \kappa + \gamma_1 \end{pmatrix}. \tag{A.7}$$

In the weak lensing regime and under the Born approximation, A is a symmetric matrix by definition and ω vanishes, we will ignore it from here on out. Intuitively, A tells you how a small patch in the sky transforms due to lensing. If we change the unlensed direction of a light source by $\delta\hat{\mathbf{n}}$, then the corresponding change in direction in the lensed image can be calculated as

$$\hat{\mathbf{n}} + \delta\hat{\mathbf{n}} \to \hat{\mathbf{n}} + \delta\hat{\mathbf{n}} + \mathbf{d}(\hat{\mathbf{n}} + \delta\hat{\mathbf{n}}) = \hat{\mathbf{n}} + \mathbf{d}(\hat{\mathbf{n}}) + \delta\hat{\mathbf{n}} + A_{ij}(\delta\hat{\mathbf{n}})_j. \tag{A.8}$$

For an image of the sky, A_{ij} thus introduces distortion. Note that $|A_{ij}| = (1-\kappa)^2 + \omega^2 - |\gamma|^2 = 1 - 2\kappa + O(\kappa^2, \gamma^2, \omega^2)$. We can thus interpret κ as telling us about the overall magnification of the source. The γ_i represents the area-preserving distortion, i.e. stretching and squeezing in a specific direction.

We can relate κ and γ directly to the lensing potential as

$$\kappa = \frac{1}{2}\nabla^2\psi, \quad \gamma_1 = \frac{1}{2}(\partial_{n_1}^2 - \partial_{n_2}^2)\psi, \quad \gamma_2 = \partial_{n_1}\partial_{n_2}\psi. \tag{A.9}$$

It is shown in appendix D that

$$\gamma := \gamma_1 + i\gamma_2 = \frac{1}{2}\eth_1(\eth_0\psi) \tag{A.10}$$

where the spin raising operator, $\eth_s$ acts on a spin s function defined on S^2 to create a spin $s+1$ function. $\eth_s$ can be written in spherical coordinates (θ, ϕ) as[6]

$$\eth_s = -\sin^s\theta(\partial_\theta + \frac{i}{\sin\theta})\frac{1}{\sin^s\theta}. \tag{A.11}$$

In this context, a spin s function refers to a function ${}_sf(\theta,\phi)$ that transforms under any rotation of coordinates by picking up a phase factor $e^{is\alpha}$, with α the angle of the rotation, i.e.

$$f'(\theta',\phi') = e^{is\alpha}f(\theta,\phi). \tag{A.12}$$

Shear is thus a spin 2 function, which can be checked by noting that rotating a galaxy image stretched and squeezed through weak lensing by 180 degrees gives the same stretching and squeezing, i.e. the same shear.

The spherical harmonics are eigenfunctions of ∇^2 and the spin raising and lowering operators. Using this property, the corresponding relations in spherical harmonic space can be shown to be

$$\kappa_{lm} = \frac{l(l+1)}{2}\psi_{lm}, \quad \gamma_{lm} = \frac{\sqrt{(l-1)l(l+1)(l+2)}}{2}\psi_{lm}.$$

B Weak Lensing Statistics

B.1 Lensing Potential Power spectrum

The lensing potential can be decomposed into spherical harmonics as

$$\psi(\hat{\mathbf{n}}) = \sum_{\ell m}\psi_{\ell m}Y_{\ell m}(\hat{\mathbf{n}}). \tag{B.1}$$

On the other hand, consider the decomposition of Ψ in Fourier modes with the Fourier convention $\Psi(\mathbf{x},\eta) = \int \frac{\mathrm{d}^3\mathbf{k}}{(2\pi)^3}\Psi(\mathbf{k},\eta)e^{i\mathbf{k}\cdot\mathbf{x}}$,

$$\psi(\hat{\mathbf{n}}) = -2\int_0^{\chi_*}\mathrm{d}\chi W(\chi)\int\frac{\mathrm{d}^3\mathbf{k}}{(2\pi)^3}\Psi(\mathbf{k},\eta_0-\chi)e^{i\mathbf{k}\cdot\hat{\mathbf{n}}\chi}. \tag{B.2}$$

We can then relate the multipole modes of ψ to the Fourier modes of Ψ through

$$\psi_{lm} = \langle Y_\ell^m|\psi\rangle = \int \mathrm{d}^2\hat{\mathbf{n}}Y_\ell^m(\hat{\mathbf{n}})^*\psi(\hat{\mathbf{n}}) \tag{B.3}$$

$$= -2\int \mathrm{d}^2\hat{\mathbf{n}}Y_l^m(\hat{\mathbf{n}})^*\int_0^{\chi_*}\mathrm{d}\chi W(\chi)\int\frac{\mathrm{d}^3\mathbf{k}}{(2\pi)^3}\Psi(\mathbf{k},\eta_0-\chi)e^{i\mathbf{k}\cdot\hat{\mathbf{n}}\chi} \tag{B.4}$$

Now define the power spectrum as

$$\langle\Psi(\mathbf{k},\eta)\Psi(\mathbf{k}',\eta')\rangle = \frac{2\pi^2}{k^3}P_\Psi(k,\eta,\eta')\delta(\mathbf{k}+\mathbf{k}'), \tag{B.5}$$

[6] We use the physics convention for the definition of θ and ϕ here.

with η denoting the conformal time. This gives

$$\langle\psi(\hat{\mathbf{n}})\psi(\hat{\mathbf{n}}')\rangle = 4\int_0^{\chi_*} \mathrm{d}\chi \int_0^{\chi_*} \mathrm{d}\chi' W(\chi)W(\chi') \int \frac{\mathrm{d}^3\mathbf{k}}{(2\pi)^6}\frac{2\pi^2}{k^3} P_\psi(k, \eta_0-\chi, \eta_0-\chi') e^{i\mathbf{k}\cdot\hat{\mathbf{n}}\chi} e^{-i\mathbf{k}\cdot\hat{\mathbf{n}}'\chi'}, \tag{B.6}$$

where we used that $\eta = \eta_0 - \chi$ along the unperturbed photon path (this is known as the Born approximation), with η_0 the time at which the light ray hits Earth. We can use the result

$$e^{i\mathbf{k}\cdot\hat{\mathbf{n}}\chi} = 4\pi\sum_{\ell m} i^\ell j_\ell(k\chi) Y_\ell^m(\hat{\mathbf{n}})^* Y_\ell^m(\hat{\mathbf{k}}) = 4\pi\sum_{\ell m} i^\ell j_\ell(k\chi) Y_\ell^m(\hat{\mathbf{n}}) Y_\ell^m(\hat{\mathbf{k}})^*, \tag{B.7}$$

where j_l is the spherical Bessel function, to rewrite the above equation. Using both versions of the identity above, we immediately get a factor $Y_\ell^m(\hat{\mathbf{k}})Y_{\ell'}^{m'}(\hat{\mathbf{k}})^*$ in our integral. We can factor the differential element of $\mathrm{d}^3\mathbf{k}$ into a radial and angular part as $k^2\mathrm{d}k\mathrm{d}^2\Omega_k$, with Ω_k the solid angle, to apply the orthonormality condition of the spherical harmonics. Note that we take the same sequence of steps a number of times in other parts of the derivations of the lensing spectra. We thus obtain

$$\langle\psi(\hat{\mathbf{n}})\psi(\hat{\mathbf{n}}')\rangle = 4(4\pi)^2 \sum_{ll'mm'} i^{l-l'} \int_0^{\chi_*} \mathrm{d}\chi \int_0^{\chi_*} \mathrm{d}\chi' W(\chi)W(\chi') \tag{B.8}$$

$$\times \int \frac{k^2\mathrm{d}k}{(2\pi)^6}\frac{2\pi^2}{k^3} j_\ell(k\chi) j_{\ell'}(k\chi') P_\psi(k, \eta_0-\chi, \eta_0-\chi') Y_{\ell m}(\hat{\mathbf{n}}) Y_{\ell' m'}(\hat{\mathbf{n}}')^* \delta_{\ell\ell'}\delta_{mm'}. \tag{B.9}$$

The angular power spectrum is defined similarly to the power spectrum, i.e.

$$\langle\psi_{\ell m}\psi^*_{\ell' m'}\rangle = \delta_{\ell\ell'}\delta_{mm'}C_\ell^\psi. \tag{B.10}$$

Note that the correlation is independent of m and m'. We can thus read from equation B.9 that

$$C_l^\psi = 4(4\pi)^2 \int_0^{\chi_*} \mathrm{d}\chi \int_0^{\chi_*} \mathrm{d}\chi' W(\chi)W(\chi') \int \frac{k^2\mathrm{d}k}{(2\pi)^6}\frac{2\pi^2}{k^3} j_\ell(k\chi) j_\ell(k\chi') P_\psi(k, \eta_0-\chi, \eta_0-\chi'), \tag{B.11}$$

which can be simplified to

$$C_\ell^\psi = \frac{2}{\pi^2}\int_0^{\chi_*} \mathrm{d}\chi \int_0^{\chi_*} \mathrm{d}\chi' W(\chi)W(\chi') \int k^2\mathrm{d}k j_\ell(k\chi) j_\ell(k\chi') \frac{P_\psi(k, \eta_0-\chi, \eta_0-\chi')}{k^3}. \tag{B.12}$$

To further evaluate the integral we will make the Limber approximation. The Bessel functions peak sharply at $l = x$[7], with the peak being increasingly sharp for higher l. Similarly to $\delta(x - x_0)f(x) = \delta(x - x_0)f(x_0)$, we thus take $j_l(k\chi)f(k) \approx j_l(k\chi)f(l/\chi)$. The Bessel functions satisfy an orthogonality condition,

$$\int k^2\mathrm{d}k j_\ell(k\chi) j_\ell(k\chi') = \frac{\pi}{2\chi^2}\delta(\chi - \chi'). \tag{B.13}$$

In combination with the Limber approximation we thus find

$$\int k^2\mathrm{d}k j_\ell(k\chi) j_\ell(k\chi') f(k) \approx \frac{\pi}{2\chi^2}\delta(\chi - \chi') f(\ell/\chi). \tag{B.14}$$

It allows us to write the Limber-approximate angular spectrum as

$$C_\ell^\psi = \frac{2}{\pi^2}\int_0^{\chi_*} \mathrm{d}\chi \int_0^{\chi_*} \mathrm{d}\chi' W(\chi)W(\chi') \frac{\pi}{2\chi^2}\delta(\chi - \chi')\frac{\chi^3}{\ell^3} P_\psi(\ell/\chi, \eta_0-\chi, \eta_0-\chi') \tag{B.15}$$

$$= \frac{1}{\ell^3\pi}\int_0^{\chi_*} \chi\mathrm{d}\chi W(\chi)^2 P_\psi(\ell/\chi, \eta_0-\chi, \eta_0-\chi). \tag{B.16}$$

[7]Some sources use $x \approx l + 1/2$ instead, which is slightly more accurate for larger scales (low l) and slightly less accurate for smaller scales.

B.2 Lensing potential bispectrum

The derivation of the bispectrum proceeds similarly to that of the power spectrum. We aim to compute the bispectrum of the lensing potential fields of 3 (possibly distinct sources), ψ_1, ψ_2, ψ_3.

$$\langle(\psi_1)_{\ell_1 m_1}(\psi_2)_{\ell_2 m_2}(\psi_3)_{\ell_3 m_3}\rangle = \prod_i \left(-2\int \mathrm{d}^2\hat{\mathbf{n}}_i (Y^{m_i}_{\ell_i}(\hat{\mathbf{n}}_i))^* \int_0^{\chi_*} \mathrm{d}\chi_i W_i(\chi_i) \int \frac{\mathrm{d}^3\mathbf{k}_i}{(2\pi)^3} e^{i\mathbf{k}_i\cdot\hat{\mathbf{n}}_i\chi_i}\right)$$
$$\times\langle\prod_i \Psi(\mathbf{k}_i, \eta_0-\chi_i)\rangle.$$

Defining the bispectrum of the gravitational potential as

$$\langle \prod_{i=1,2,3} \Psi(\mathbf{k}_i, \eta_0-\chi_i)\rangle = (2\pi)^3\delta(\mathbf{k}_1+\mathbf{k}_2+\mathbf{k}_3)B^\Psi(\{k_i\},\{\eta_0-\chi_i\}),$$

we rewrite the lensing potential bispectrum as

$$\langle(\psi_1)_{\ell_1 m_1}(\psi_2)_{\ell_2 m_2}(\psi_3)_{\ell_3 m_3}\rangle = \prod_i \left(-2\int \mathrm{d}^2\hat{\mathbf{n}}_i (Y^{m_i}_{\ell_i}(\hat{\mathbf{n}}_i))^* \int_0^{\chi_*} \mathrm{d}\chi_i W_i(\chi_i) \int \frac{\mathrm{d}^3\mathbf{k}_i}{(2\pi)^3} e^{i\mathbf{k}_i\cdot\hat{\mathbf{n}}_i\chi_i}\right)$$
$$\times(2\pi)^3\delta(\mathbf{k}_1+\mathbf{k}_2+\mathbf{k}_3)B^\Psi(\{k_i\},\{\eta_0-\chi_i\}).$$

Now using equation B.7 to rewrite the complex exponential:

$$\langle(\psi_1)_{\ell_1 m_1}(\psi_2)_{\ell_2 m_2}(\psi_3)_{\ell_3 m_3}\rangle$$
$$= \prod_i \left(-2\int \mathrm{d}^2\hat{\mathbf{n}}_i (Y^{m_i}_{\ell_i}(\hat{\mathbf{n}}_i))^* \int_0^{\chi_*} \mathrm{d}\chi_i W_i(\chi_i) \int \frac{\mathrm{d}^3\mathbf{k}_i}{(2\pi)^3} 4\pi \sum_{\ell m} i^\ell j_l(k_i\chi_i) Y^m_\ell(\hat{\mathbf{n}}_i) Y^m_\ell(\hat{\mathbf{k}}_i)^*\right)$$
$$\times(2\pi)^3\delta(\mathbf{k}_1+\mathbf{k}_2+\mathbf{k}_3)B^\Psi(\{k_i\},\{\eta_0-\chi_i\})$$
$$= \left[\prod_i \left(-2\int_0^{\chi_*} \mathrm{d}\chi_i W_i(\chi_i) \int \frac{\mathrm{d}^3\mathbf{k}_i}{(2\pi)^3} 4\pi i^{\ell_i} j_{\ell_i}(k_i\chi_i) Y^{m_i}_{\ell_i}(\hat{\mathbf{k}}_i)^*\right)\right](2\pi)^3\delta(\mathbf{k}_1+\mathbf{k}_2+\mathbf{k}_3)B^\Psi(\{k_i\},\{\eta_0-\chi_i\}).$$

We can write the 3D Dirac delta function in terms of spherical harmonics as

$$\delta(\mathbf{k}_1+\mathbf{k}_2+\mathbf{k}_3) = 8\int \mathrm{d}^3\mathbf{x} \prod_{i=1,2,3}\left(\sum_{\ell_j m_j} i^{\ell_j} j_{\ell_j}(k_i x) Y^{m_j}_{\ell_j}(\hat{\mathbf{k}}_i) Y^{m_j}_{\ell_j}(\hat{\mathbf{x}})^*\right).$$

This results in

$$\langle(\psi_1)_{\ell_1 m_1}(\psi_2)_{\ell_2 m_2}(\psi_3)_{\ell_3 m_3}\rangle = \prod_i \left(-2\int_0^{\chi_*} \mathrm{d}\chi_i W_i(\chi_i) \int \frac{\mathrm{d}^3\mathbf{k}_i}{(2\pi)^3} 4\pi i^{\ell_i} j_{\ell_i}(k_i\chi_i) Y^{m_i}_{\ell_i}(\hat{\mathbf{k}}_i)^*\right)$$
$$\times(2\pi)^3 8\int \mathrm{d}^3\mathbf{x} \prod_i \left(\sum_{\ell m} i^\ell j_\ell(k_i x) Y^m_\ell(\hat{\mathbf{k}}_i) Y^m_\ell(\hat{\mathbf{x}})^*\right) B^\Psi(\{k_i\},\{\eta_0-\chi_i\})$$
$$= (2\pi)^3 8\int \mathrm{d}^3\mathbf{x} \prod_i \left(-2\int_0^{\chi_*} \mathrm{d}\chi_i W_i(\chi_i) \int \frac{k_i^2 \mathrm{d}k_i}{(2\pi)^3} 4\pi(-1)^{\ell_i} j_{\ell_i}(k_i\chi_i) j_{\ell_i}(k_i x) Y^{m_i}_{\ell_i}(\hat{\mathbf{x}})^*\right) B^\Psi(\{k_i\},\{\eta_0-\chi_i\})$$

The angular part of the $\mathbf{x}$ integral can be evaluated using the identity

$$\int \mathrm{d}\Omega_{\hat{n}}\, Y^*_{\ell_1 m_1}(\hat{x}) Y^*_{\ell_2 m_2}(\hat{n}) Y^*_{\ell_3 m_3}(\hat{n}) = (-1)^{m_1+m_2+m_3}\int \mathrm{d}\Omega_{\hat{n}}\, Y_{\ell_1 -m_1}(\hat{n}) Y_{\ell_2 -m_2}(\hat{n}) Y_{\ell_3 -m_3}(\hat{n})$$
$$= (-1)^{m_1+m_2+m_3}\sqrt{\frac{(2\ell_1+1)(2\ell_2+1)(2\ell_3+1)}{4\pi}} \begin{pmatrix}\ell_1 & \ell_2 & \ell_3\\ 0 & 0 & 0\end{pmatrix}\begin{pmatrix}\ell_1 & \ell_2 & \ell_3\\ -m_1 & -m_2 & -m_3\end{pmatrix} \equiv A^{\mathbf{m}}_{\mathbf{l}},$$

giving

$$\langle(\psi_1)_{\ell_1 m_1}(\psi_2)_{\ell_2 m_2}(\psi_3)_{\ell_3 m_3}\rangle = (2\pi)^3 8 A_{\rm I}^{\mathbf{m}} \int x^2 \mathrm{d}x \prod_i \left(-2\int_0^{\chi_*} \mathrm{d}\chi_i W_i(\chi_i) \int \frac{k_i^2 \mathrm{d}k_i}{(2\pi)^3} 4\pi(-1)^{\ell_i} j_{\ell_i}(k_i\chi_i) j_{\ell_i}(k_i x)\right)$$
$$\times B^{\Psi}(\{k_i\}, \{\eta_0 - \chi_i\}).$$

Now applying the Limber approximation again:

$$\langle(\psi_1)_{\ell_1 m_1}(\psi_2)_{\ell_2 m_2}(\psi_3)_{\ell_3 m_3}\rangle = (2\pi)^3 8 A_{\rm I}^{\mathbf{m}} \int x^2 \mathrm{d}x \prod_i \left(-2\int_0^{\chi_*} \mathrm{d}\chi_i W_i(\chi_i) \frac{1}{(2\pi)^3} \frac{\pi}{2\chi_i^2} \delta(x-\chi_i) 4\pi(-1)^{\ell_i}\right)$$
$$\times B^{\Psi}(\{\ell_i/\chi_i\}, \{\eta_0 - \chi_i\})$$
$$= (2\pi)^3 8 A_{\rm I}^{\mathbf{m}} \int \chi^2 \mathrm{d}\chi \prod_i \left(-2W_i(\chi) \frac{1}{(2\pi)^3} \frac{\pi}{2\chi^2} 4\pi(-1)^{\ell_i}\right) B^{\Psi}(\{\ell_i/\chi\}, \eta_0 - \chi).$$

Finally, we aim to rewrite the above in terms of the angular bispectrum of the lensing potential.

The definition for the bispectrum of any set of randomly distributed spherical harmonic components $X^k_{\ell m}$ is [11]

$$\langle(X_1)_{\ell_1 m_1}(X_2)_{\ell_2 m_2}(X_3)_{x_3 m_3}\rangle = \begin{pmatrix} \ell_1 & \ell_2 & \ell_3 \\ m_1 & m_2 & m_3 \end{pmatrix} B^{X_1 X_2 X_3}_{\ell_1 \ell_2 \ell_3}.$$

Note the independence on m_i, this necessarily follows from statistical isotropy. If $m_1+m_2+m_3 \neq 0$, the associated Wigner-3j symbol vanishes and the bispectrum is set to zero. Also note that in this definition we have immediately generalized to include cross correlation between different fields X_1, X_2, X_3. This is relevant when we look at cross-correlations between CMB and galaxy lensing. 6758 Using the above definition and the symmetry property

$$\begin{pmatrix} \ell_1 & \ell_2 & \ell_3 \\ -m_1 & -m_2 & -m_3 \end{pmatrix} = (-1)^{\ell_1+\ell_2+\ell_3} \begin{pmatrix} \ell_1 & \ell_2 & \ell_3 \\ m_1 & m_2 & m_3 \end{pmatrix},$$

we find

$$B^{\psi_1\psi_2\psi_3}_{\ell_1\ell_2\ell_3} = (-1)^{\ell_1+\ell_2+\ell_3} \sqrt{\frac{(2\ell_1+1)(2\ell_2+1)(2\ell_3+1)}{4\pi}} \begin{pmatrix} \ell_1 & \ell_2 & \ell_3 \\ 0 & 0 & 0 \end{pmatrix} (2\pi)^3 8$$
$$\times \int \chi^2 \mathrm{d}\chi \prod_i \left(-2W_i(\chi, \chi_*) \frac{1}{(2\pi)^3} \frac{\pi}{2\chi^2} 4\pi(-1)^{\ell_i}\right) B^{\Psi}(\{\ell_i/\chi\}, \{\eta_0 - \chi\}),$$

where we were able to drop the $(-1)^{m_1+m_2+m_3}$ factor due to the bispectrum vanishing if that sum does not equal 0, as mentioned earlier. When all m_i equal zero, the Wigner 3j-symbol gains a number of useful properties In particular, it vanishes if $\ell_1 + \ell_2 + \ell_3$ is odd, meaning we can drop the $(-1)^{\ell_1+\ell_2+\ell_3}$ factor. Additionally cancelling common factors then gives

$$B^{\psi_1\psi_2\psi_3}_{\ell_1\ell_2\ell_3} = -\sqrt{\frac{(2\ell_1+1)(2\ell_2+1)(2\ell_3+1)}{4\pi}} \begin{pmatrix} \ell_1 & \ell_2 & \ell_3 \\ 0 & 0 & 0 \end{pmatrix} 8 \int \frac{\mathrm{d}\chi}{\chi^4} W_1(\chi) W_2(\chi) W_3(\chi) B^{\Psi}(\{l_i/\chi\}, \eta_0 - \chi). \tag{B.17}$$

B.3 Gravitational potential spectra in terms of matter spectra

We can rewrite equations B.16 and B.17 in terms of the matter spectra instead of the ψ spectra using the poisson equation. This allows us to numerically evaluate these lensing spectra using CAMB. The density contrast is defined as

$$\delta(\mathbf{x}) := \frac{\rho(\mathbf{x}) - \bar{\rho}}{\bar{\rho}}, \tag{B.18}$$

and the matter spectra are defined in terms of the fourier transformed density contrast $\delta(\mathbf{k})$ as

$$\begin{aligned}\langle \delta(\mathbf{k},\eta)\delta(\mathbf{k}',\eta)^*\rangle &= (2\pi)^3\delta(\mathbf{k}-\mathbf{k}')P^\delta(\mathbf{k},\eta),\\ \langle \delta(\mathbf{k}_1,\eta)\delta(\mathbf{k}_2,\eta)\delta(\mathbf{k}_3,\eta)\rangle &= (2\pi)^3\delta(\mathbf{k}_1+\mathbf{k}_2+\mathbf{k}_3)B^\delta(k_1,k_2,k_3,\eta).\end{aligned}$$

The mean matter density of the universe, $\bar{\rho}$ is given as

$$\bar{\rho}(\eta) = \frac{3\Omega_m H_0^2}{8\pi G}\frac{1}{a(\eta)^3},$$

where $a(\eta)$ is the only time dependent factor on the right hand side. The poisson equation relates Ψ to the density contrast as [13]

$$\nabla^2\Psi(\mathbf{x}) = 4\pi G a^2\left(\frac{3\Omega_m H_0^2}{8\pi G}\frac{1}{a^3}\right)\delta(\mathbf{x}) = \frac{3\Omega_m H_0^2}{2}\frac{1}{a}\delta(\mathbf{x}) \implies \Psi(k,\eta) = -\frac{3\Omega_m H_0^2}{2}\frac{1}{a}\frac{\delta(k,\eta)}{k^2}, \tag{B.19}$$

where $\Psi(k,\eta)$ and $\delta(k,\eta)$ are functions in Fourier space. For the power- and bispectra we find

$$\begin{aligned}\langle \Psi(\mathbf{k},\eta)\Psi^*(\mathbf{k}',\eta)\rangle = \frac{2\pi^2}{k^3}C^\Psi(k,\eta)\delta(\mathbf{k}-\mathbf{k}') &\implies C^\Psi(k,\eta) = \frac{1}{k}(9\Omega_m^2 H_0^4\pi)\frac{1}{a^2}C^\delta(k,\eta),\\ \langle \Psi(\mathbf{k}_1,\eta)\Psi(\mathbf{k}_2,\eta)\Psi(\mathbf{k}_3,\eta)\rangle &= -(2\pi)^3\delta(\mathbf{k}_1+\mathbf{k}_2+\mathbf{k}_3)B^\Psi(k_1,k_2,k_3,\eta)\\ \implies B^\Psi(k_1,k_2,k_3,\eta) &= -\frac{1}{k_1^2k_2^2k_3^2}\left(\frac{3\Omega_m H_0^2}{2}\right)^3\frac{1}{a^3}B^\delta(\{k_i\},\eta).\end{aligned}$$

Finally, we obtain:

$$\boxed{\begin{aligned}C_\ell^{\psi_X\psi_Y} &= \frac{9}{\ell^4}\Omega_m^2 H_0^4\int_0^{\chi_*}\chi^2 \mathrm{d}\chi a(\eta_0-\chi)^{-2}W_X(\chi)W_Y(\chi)P^\delta(\ell/\chi,\eta_0-\chi),\\ B^{\psi_X\psi_Y\psi_Z}_{\ell_1\ell_2\ell_3} &= \sqrt{\frac{(2\ell_1+1)(2\ell_2+1)(2\ell_3+1)}{4\pi}}\begin{pmatrix}\ell_1 & \ell_2 & \ell_3\\ 0 & 0 & 0\end{pmatrix}\frac{27}{\ell_1^2\ell_2^2\ell_3^2}\Omega_m^3 H_0^6\\ &\quad\times\int\chi^2\mathrm{d}\chi a(\eta_0-\chi)^{-3}W_X(\chi)W_Y(\chi)W_Z(\chi)B^\delta(\{\ell_i/\chi\},\eta_0-\chi).\end{aligned}}$$

C Fisher Matrix Analysis

C.1 Determing uncertainty in experimental parameters

The Fisher matrix formalism is used to find a lower bound on the constraints we can place on experimental parameters. It combines the Cramer-Rao Inequality [9] with the assumption that we

have unbiased estimators following a gaussian distribution [13]. In particular, denoting the Fisher matrix by $F_{\theta_i\theta_j}$, the parameters as θ_i, and their estimators as $\hat{\theta}_i$, it can be shown that

$$\mathrm{Var}(\hat{\theta}_i) \geq \left(F^{-1}\right)_{\theta_i\theta_i}. \tag{C.1}$$

In the case of n measurements whose outcomes are realizations of random variables x_i, each with associated mean μ_{x_i}, the Fisher matrix is given as

$$F_{\theta_i\theta_j} := \sum_{p,q=1}^{n} \frac{\partial \mu_{x_p}}{\partial \theta_i}(\tilde{\theta}_k)(\mathrm{Cov}^{-1})_{x_p x_q}(\tilde{\theta}_k)\frac{\partial \mu_{x_q}}{\partial \theta_j}(\tilde{\theta}_k), \tag{C.2}$$

where Cov is the covariance matrix associated with the random vector $(x_1, ..., x_n)$, $\mathrm{Cov}_{x_p x_q} := \mathrm{Cov}(x_p, x_q)$. The derivative of the mean measurement outcomes and measurement covariances will in general depend on the true, unknown, values of the experimental parameters. We therefore evaluate these quantities with for our best guess of the experimental parameters given some outside information. These are known as the "fiducial" values.

C.2 Fisher matrices for power- and bispectra with multiple tracers

For power spectra, the definition of the Fisher matrix gives

$$F_{\alpha\beta} = \sum_{l_{min}\leq\ell,\ell'\leq\ell_{max}} \sum_{[XY][X'Y']} \partial_\alpha C_\ell^{XY} \left(\mathrm{Cov}^{-1}\right)_{\ell,\ell'}^{XY,X'Y'} \partial_\beta C_{\ell'}^{X'Y'}.$$

Here the covariance matrix is given as

$$\mathrm{Cov}_{\ell,\ell'}^{XY,X'Y'} = \langle \hat{C}_\ell^{XY} \hat{C}_{\ell'}^{X'Y'} \rangle.$$

The estimator of the power- or bi-spectrum is the product of the estimators of the appropriate tracers, e.g. $\hat{C}_\ell^{XY} = \hat{X}(\ell)\hat{Y}(\ell)$. The sum over $[XY]$ and $[X'Y']$ denotes a sum over possible tracer combinations *without* counting permutations of tracer configuration. This is because permutations are not distinct signals, i.e. $\hat{X}(\ell)\hat{Y}(\ell) = \hat{Y}(\ell)\hat{X}(\ell)$. In fact, if we were to count these permutations as distinct signals we would get identical columns and/or rows in our covariance matrix making inversion impossible:

$$\langle \hat{X}(\ell)\hat{Y}(\ell)\hat{X}'(\ell')\hat{Y}'(\ell')\rangle = \langle \hat{Y}(\ell)\hat{X}(\ell)\hat{X}'(\ell')\hat{Y}'(\ell')\rangle, \quad \forall X', Y', \ell'.$$

To evaluate the covariance matrix we again assume that the estimators are Gaussian distributed so that we can apply a wick contraction, as is commonly done [36]. In this case we get

$$\mathrm{Cov}_{\ell,\ell'}^{XY,X'Y'} = \frac{1}{2\ell+1}\delta_{\ell\ell'}\left(\tilde{C}_\ell^{XX'}\tilde{C}_\ell^{YY'} + \tilde{C}_\ell^{XY'}\tilde{C}_\ell^{YX'}\right).$$

Two remarks are in order.

1. By definition
$$\langle X_{\ell m} X'_{\ell' m'}\rangle = (2\pi)^3 \delta_{\ell\ell'}\delta_{mm'} C_\ell^{XX'},$$
so you can average over the measurements done for different values of m, i.e. $X_{\ell(-\ell)}$, $X_{\ell(-\ell+1)}$, $\cdots$, $X_{\ell(\ell-1)}$, $X_{\ell\ell}$. This results in the $(2\ell+1)^{-1}$ factor in the power spectrum covariance.

2. The tilde is used to denote the power spectrum as calculated earlier plus the noise power spectrum, $N_\ell^{XX'}$, which is the power spectrum of the noise associated with the estimator of the field. This is where experimental noise is incorporated into the calculation.

Under the Gaussian approximation, the covariance matrix vanishes except for 3×3 block matrices (in the case of 2 tracers) on the diagonal. The fisher matrix is then

$$F_{\alpha\beta} = \sum_\ell \sum_{[XY][X'Y']} \partial_\alpha C_\ell^{XY} \left(\mathrm{Cov}_\ell^{-1}\right)^{XY,X'Y'} \partial_\beta C_\ell^{X'Y'}.$$

Cov_ℓ^{-1} here denotes the inverse of the block matrix at l.

Next, we consider the Fisher matrix for bispectra measurements.

$$F_{\alpha\beta} = \sum_{\text{distinct signals}} \sum_{\text{distinct signals prime}} B^{XYZ}_{\ell_1\ell_2\ell_3} \left(\mathrm{Cov}^{-1}\right)^{XYZ,X'Z'Y'}_{\ell_1\ell_2\ell_3,\ell_1'\ell_2'\ell_3'} B^{X'Y'Z'}_{\ell_1'\ell_2'\ell_3'}.$$

Counting only distinct signals requires more care compared to the power spectra. The rule is that $B^{XYZ}_{\ell_1\ell_2\ell_3}$ and $B^{X'Y'Z'}_{\ell_1'\ell_2'\ell_3'}$ are not distinct signals if there exists a permutation σ that simultaniously maps $X'Y'Z'$ to XYZ and $\ell_1'\ell_2'\ell_3'$ to $\ell_1\ell_2\ell_3$. It turns out that we can write a sum over distinct signals explicitly as

$$\sum_{\text{distinct signals}} = \underbrace{\sum_{\ell_1=\ell_2=\ell_3} \sum_{[XYZ]}}_{\text{sum 1}} + \underbrace{\sum_{\ell_1=\ell_2\neq\ell_3} \sum_{[XY]Z}}_{\text{sum 2}} + \underbrace{\sum_{\ell_1<\ell_2<\ell_3} \sum_{XYZ}}_{\text{sum 3}}.$$

With the same definition again for the $[\cdot]$ notation. For example:

$$\{[XY]Z | X, Y, Z \in \{\psi_\kappa, \psi_\gamma\}\} = \{\psi_\kappa\psi_\kappa\psi_\kappa, \psi_\kappa\psi_\gamma\psi_\kappa, \psi_\gamma\psi_\gamma\psi_\kappa, \psi_\kappa\psi_\kappa\psi_\gamma, \psi_\kappa\psi_\gamma\psi_\gamma, \psi_\gamma\psi_\gamma\psi_\gamma\}.$$

It follows to show that the sets that these sums sum over form a partition of the set of all distinct signals. Clearly all 3 sets are pairwise disjoint (no common elements) because of the criteria for the l_i's. To show that their union covers the set of distinct signals, start by considering an arbitrary signal. Its l configuration will trivially correspond to exactly one of the three sums. If it is sum 1, then we are free to permute the XYZ's by virtue of the l's being identical so we will be able to match the XYZ configuration to one of the elements of $\{\{XYZ\}\}$. Similarly, if the l configuration corresponds to sum 2, then we are free to permute the XY configuration to match with one of the elements of $\{\{XY\}Z\}$. The Z value does not matter because any Z value is accounted for. For sum 3 we can argue that we can switch around the order of the l's to satisfy $\ell_1 < l2 < l3$ and the corresponding XYZ configuration will be accounted for in sum 3 because all XYZ combinations are counted. Finally, it is simple to verify that no distinct signal is counted more than once within each sum.

To calculate the elements of the covariance matrix consider the following. Every element of the Fisher matrix can be seen as an inner product weighted by the inverse covariance matrix. We can choose how we order the vectors[8]. We organize the vectors according to the sum 1, 2, and 3 parts first. Then by l configuration. Within each l configuration we can choose any ordering for the XYZ

[8]The entries are the derivatives of the bispectra

configurations. The covariance matrix now becomes a block matrix with each block corresponding to an l_i and l_i' configuration. When wick contracting using the gaussian approximation, every block matrix where $(\ell_1, \ell_2, \ell_3) \neq (\ell_1', \ell_2', \ell_3')$ vanishes. It can then be shown that the entries of each block matrix are given as

$$(\mathrm{Cov}_{\ell_1\ell_2\ell_3})^{XYZ,X'Y'Z'} = \tilde{C}_{\ell_1}^{XX'}\tilde{C}_{\ell_2}^{YY'}\tilde{C}_{\ell_3}^{ZZ'} + \delta_{\ell_1\ell_2}\tilde{C}_{\ell_1}^{XY'}\tilde{C}_{\ell_2}^{YX'}\tilde{C}_{\ell_3}^{ZZ'} + \delta_{\ell_2\ell_3}\tilde{C}_{\ell_1}^{XX'}\tilde{C}_{\ell_2}^{YZ'}\tilde{C}_{\ell_3}^{ZX'}$$
$$+\delta_{\ell_3\ell_1}\tilde{C}_{\ell_1}^{XZ'}\tilde{C}_{\ell_2}^{YY'}\tilde{C}_{\ell_3}^{ZX'} + \delta_{\ell_1\ell_2}\delta_{\ell_2\ell_3}\left(\tilde{C}_{\ell_1}^{XY'}\tilde{C}_{\ell_2}^{YZ'}\tilde{C}_{\ell_3}^{ZX'} + \tilde{C}_{\ell_1}^{XZ'}\tilde{C}_{\ell_2}^{YX'}\tilde{C}_{\ell_3}^{ZY'}\right).$$

With our ordering this means that the covariance matrix is again a diagonal block matrix, now with blocks of size 4×4 (sum 1), 6×6 (sum 2), and 8×8 (sum 3).

C.3 Explicit form for inverse covariance matrix

The Fisher matrix above can be significantly simplified and written as

$$F_{\alpha\beta} = \sum_{\ell_1\leq\ell_2\leq\ell_3} \frac{\mathcal{P}_{\ell_1\ell_2\ell_3}}{6} \sum_{XYZ}\sum_{X'Y'Z'} \partial_\alpha B_{\ell_1\ell_2\ell_3}^{XYZ} (\tilde{C}^{-1})_{\ell_1}^{XX'} (\tilde{C}^{-1})_{\ell_2}^{YY'} (\tilde{C}^{-1})_{\ell_3}^{ZZ'} \partial_\beta B_{\ell_1\ell_2\ell_3}^{X'Y'Z'}$$

where, in the case of two tracers,

$$C_l := \begin{pmatrix} \tilde{C}_l^{\psi_1\psi_1} & \tilde{C}_l^{\psi_1\psi_2} \\ \tilde{C}_l^{\psi_1\psi_2} & \tilde{C}_l^{\psi_2\psi_2} \end{pmatrix}$$

and $\mathcal{P}_{\ell_1\ell_2\ell_3}$ is defined as the number of distinct permutations that can be made with $\ell_1\ell_2\ell_3$. This form was, for example, used in [21][9].

To show that the above is the same as the formula for the Fisher matrix given earlier, first parition the sum in the same way and collect all terms that fit in the different categories.

$$F_{\alpha\beta} = \sum_{\ell_1=\ell_2=\ell_3} \sum_{[XYZ]} \sum_{[X'Y'Z']} \partial_\alpha B_{\ell_1\ell_2\ell_3}^{XYZ} \left(\frac{\mathcal{P}_{\ell_1\ell_2\ell_3}}{6} \sum_{d.p.XYZ} \sum_{d.p.X'Y'Z'} (\tilde{C}^{-1})_{\ell_1}^{XX'} (\tilde{C}^{-1})_{\ell_2}^{YY'} (\tilde{C}^{-1})_{\ell_3}^{ZZ'} \right) \partial_\beta B_{\ell_1\ell_2\ell_3}^{X'Y'Z'}$$
$$+ \sum_{\ell_1=\ell_2\neq\ell_3} \sum_{[XY]Z} \sum_{[X'Y']Z'} \partial_\alpha B_{\ell_1\ell_2\ell_3}^{XYZ} \left(\frac{\mathcal{P}_{\ell_1\ell_2\ell_3}}{6} \sum_{d.p.XY} \sum_{d.p.X'Y'} (\tilde{C}^{-1})_{\ell_1}^{XX'} (\tilde{C}^{-1})_{\ell_2}^{YY'} (\tilde{C}^{-1})_{\ell_3}^{ZZ'} \right) \partial_\beta B_{\ell_1\ell_2\ell_3}^{X'Y'Z'}$$
$$+ \sum_{\ell_1<\ell_2<\ell_3} \sum_{XYZ} \sum_{X'Y'Z'} \partial_\alpha B_{\ell_1\ell_2\ell_3}^{XYZ} (\tilde{C}^{-1})_{\ell_1}^{XX'} (\tilde{C}^{-1})_{\ell_2}^{YY'} (\tilde{C}^{-1})_{\ell_3}^{ZZ'} \partial_\beta B_{\ell_1\ell_2\ell_3}^{X'Y'Z'},$$

where "*d.p.*" stands for "distinct permutations". The entries above are then the entries of the inverses of the block matrices mentioned earlier. This can be checked. For example, for the $\ell_1 = \ell_2 = \ell_3$ sum the multiplication of block matrices corresponding to the same l_i configuration

[9] Note that in [21] this is based on a previous equation summing over *all* l_i (so including permutations of each configuration) which is missing a factor of 1/6.

can be written as:

$$\sum_{[X'Y'Z']}\left(\frac{\mathcal{P}_{\ell_1\ell_2\ell_3}}{6}\sum_{d.p.XYZ}\sum_{d.p.X'Y'Z'}(\tilde{C}^{-1})_l^{XX'}(\tilde{C}^{-1})_l^{YY'}(\tilde{C}^{-1})_l^{ZZ'}\right)\left(\tilde{C}_l^{X'X''}\tilde{C}_l^{Y'Y''}\tilde{C}_l^{Z'Z''}+\text{perms } X''Y''Z''\right)$$
$$=\frac{\mathcal{P}_{\ell_1\ell_2\ell_3}}{6}\left[\left(\sum_{d.p.XYZ}\sum_{X'Y'Z'}(\tilde{C}^{-1})_l^{XX'}(\tilde{C}^{-1})_l^{YY'}(\tilde{C}^{-1})_l^{ZZ'}\right)\tilde{C}_l^{X'X''}\tilde{C}_l^{Y'Y''}\tilde{C}_l^{Z'Z''}\right]+\text{perms } X''Y''Z''$$
$$=\frac{\mathcal{P}_{\ell_1\ell_2\ell_3}}{6}\sum_{d.p.XYZ}\delta_{XX''}\delta_{YY''}\delta_{ZZ''}+\text{perms } X''Y''Z''=\frac{\mathcal{P}_{\ell_1\ell_2\ell_3}}{6}\delta_{[XYZ],[X''Y''Z'']}+\text{perms } X''Y''Z''$$
$$=\delta_{[XYZ],[X''Y''Z'']}.$$

The sum over the different wick contractions will similarly cancel with the $\mathcal{P}_{\ell_1\ell_2\ell_3}/6$ factor for the $\ell_1=\ell_2\neq\ell_3$ sum. For the $\ell_1<\ell_2<\ell_3$ sum the proof is similar as well except no cancellation is required.

The same type of simplification can be made in the Fisher matrix for the power spectrum, though it doesn't offer any significant benefits compared to our current 3×3 block matrix form.

C.4 Signal to Noise Ratio (SNR)

To quantify the detectability of the lensing spectra, we introduce an overal amplitude of our signal, A, with fiducial value 1 as experimental parameter and compute F_{AA}. Obviously, $\partial_A\left(AB^{XYZ}_{\ell_1\ell_2\ell_3}\right)|_{A=1}=B^{XYZ}_{\ell_1\ell_2\ell_3}$, so we find

$$\left(\frac{S}{N}\right)^2:=F_{AA}=\sum_{XYZ,X'Y'Z'}\sum_{\ell_1\leq\ell_2\leq\ell_3}\frac{\mathcal{P}_{\ell_1\ell_2\ell_3}}{6}B^{XYZ}_{\ell_1\ell_2\ell_3}(\tilde{C}^{-1})^{XX'}_{\ell_1}(\tilde{C}^{-1})^{YY'}_{\ell_2}(\tilde{C}^{-1})^{ZZ'}_{\ell_3}B^{X'Y'Z'}_{\ell_1\ell_2\ell_3}.$$

The equation for the SNR of the power spectra is identical in form.

C.5 Fisher matrix of power- + bispectra

To compute the Fisher matrix of an experiment measuring both lensing power- and bispectra we are required to compute and invert the full covariance matrix. If we keep assuming that the measurements are close enough to Gaussian to be able to use wick contractions to a good approximation, the full covariance matrix simplifies trivially. The correlation between a power- and bispectrum estimator contains an odd (5) amount of fields and thus always vanishes. We are thus allowed to simply add the Fisher matrices of the power- and bispectra to compute the combined Fisher matrix.

D Shear equals twice spin raised lensing potential

Consider a point on S^2, (r_0,θ_0,ϕ_0), at which we observe some cosmological object. We can then define a set of cartesian coordinates $(\tilde{r},\tilde{y},\tilde{x})$ as shown in figure 7.

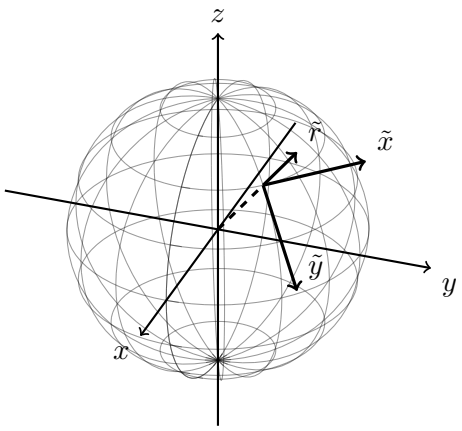

Figure 7. $(\tilde{r}, \tilde{y}, \tilde{x})$ coordinates defined for a point on the unit sphere. These act as ordinary cartesian coordinates but rotated such that, at the associated point on S^2, $\hat{\tilde{r}}$ points straight out of the unit sphere, $\hat{\tilde{y}}$ is parallel to the great arc with constant ϕ and $\hat{\tilde{x}}$ is parallel to the great arc with constant θ. These coordinates are used to define the shear and convergence in terms of the lensing potential.

Note that it is not obvious whether to define these coordinates at the point where the lensed light hits S^2 or the unlensed light hits S^2. We will assume that lensing effects are sufficiently weak that either definition works. We can then express the tilde coordinates in terms of spherical coordinates either by applying a rotation matrix or by calculating the r, θ, ϕ derivatives of (x, y, z) coordinates at (r_0, θ_0, ϕ_0) to find $\hat{\tilde{\mathbf{r}}}$, $\hat{\tilde{\boldsymbol{\theta}}}$, and $\hat{\tilde{\boldsymbol{\phi}}}$ and then take inner products. Regardless, we find

$$\tilde{r} = r\sin\theta\cos\phi\sin\theta_0\cos\phi_0 + r\sin\theta\sin\phi\sin\theta_0\sin\phi_0 + r\cos\theta\cos\theta_0, \tag{D.1}$$

$$\tilde{y} = r\sin\theta\cos\phi\cos\theta_0\cos\phi_0 + r\sin\theta\sin\phi\cos\theta_0\sin\phi_0 - r\cos\theta\sin\theta_0, \tag{D.2}$$

$$\tilde{x} = -r\sin\theta\cos\phi\sin\phi_0 + r\sin\theta\sin\phi\cos\phi_0. \tag{D.3}$$

This gives derivatives

$$\begin{aligned}
\frac{\partial}{\partial\theta} =& \left(r\cos\theta\cos\phi\sin\theta_0\cos\phi_0 + r\cos\theta\sin\phi\sin\theta_0\sin\phi_0 - r\sin\theta\cos\theta_0\right)\frac{\partial}{\partial\tilde{r}} \\
&+ \left(r\cos\theta\cos\phi\cos\theta_0\cos\phi_0 + r\cos\theta\sin\phi\cos\theta_0\sin\phi_0 + r\sin\theta\sin\theta_0\right)\frac{\partial}{\partial\tilde{y}} \\
&+ \left(-r\cos\theta\cos\phi\sin\phi_0 + r\cos\theta\sin\phi\cos\phi_0\right)\frac{\partial}{\partial\tilde{x}}. \\
\frac{\partial}{\partial\phi} =& \left(-r\sin\theta\sin\phi\sin\theta_0\cos\phi_0 + r\sin\theta\cos\phi\sin\theta_0\sin\phi_0\right)\frac{\partial}{\partial\tilde{r}} \\
&+ \left(-r\sin\theta\sin\phi\cos\theta_0\cos\phi_0 + r\sin\theta\cos\phi\cos\theta_0\sin\phi_0\right)\frac{\partial}{\partial\tilde{y}} \\
&+ \left(r\sin\theta\sin\phi\sin\phi_0 + r\sin\theta\cos\phi\cos\phi_0\right)\frac{\partial}{\partial\tilde{x}}.
\end{aligned}$$

Evaluated at our point of interest we obtain $\partial_\theta = \partial_{\tilde{y}}$ and $\partial_\phi = \sin\theta_0\partial_{\tilde{x}}$. The second-order derivatives can then be obtained using the first-order derivatives. We can immediately evaluate them at the point to get

$$\begin{aligned}
\partial^2_\phi|_{(r_0,\theta_0,\phi_0)} &= -\sin^2\theta_0\partial_{\tilde{r}} - \sin\theta_0\cos\theta_0\partial_{\tilde{y}} + \sin^2\theta_0\partial^2_{\tilde{x}}, \\
\partial_\theta\partial_\phi|_{(r_0,\theta_0,\phi_0)} &= \cos\theta_0\partial_{\tilde{x}} + \sin\theta_0\partial_{\tilde{x}}\partial_{\tilde{y}}, \\
\partial^2_\theta|_{(r_0,\theta_0,\phi_0)} &= -\partial_{\tilde{r}} + \partial^2_{\tilde{y}}.
\end{aligned}$$

Thus, at (r_0, θ_0, ϕ_0),

$$\frac{1}{2}\eth_1(\eth_0\psi) = \frac{1}{2}\sin\theta(\partial_\theta + \frac{i}{\sin\theta}\partial_\phi)(\frac{1}{\sin\theta}(\partial_\theta + \frac{1}{\sin\theta}\partial_\phi))$$
$$= \frac{\partial^2\psi}{\partial\theta^2} - \frac{\cos\theta}{\sin\theta}\frac{\partial\psi}{\partial\theta} + \frac{2i}{\sin\theta}\frac{\partial^2\psi}{\partial\theta\partial\phi} - \frac{1}{\sin^2\theta}\frac{\partial^2\psi}{\partial\phi^2} - 2i\frac{\cos\theta}{\sin^2\theta}\frac{\partial\psi}{\partial\phi}$$
$$= \frac{1}{2}(\partial_{\tilde{y}}^2 - \partial_{\tilde{x}}^2 + 2i\partial_{\tilde{x}}\partial_{\tilde{y}})\psi = \gamma_1 + i\gamma_2 = \gamma.$$

E Numerical derivative

The derivatives with respect to cosmological parameters were taken with a central difference formula, i.e.

$$f'(x) = \frac{f(x+h) - f(x-h)}{2h} + \mathcal{O}(h^2).$$

Each change of the cosmological parameters requires a recalculation of the entire cosmology, making it computationally expensive. For the approximation to be accurate a balance needs to be found between numerical errors for small h and a larger $\mathcal{O}(h^2)$ error for larger h. The h values chosen for each parameter are shown in table 4 and are similar to the values used in [28][10].

Parameter	Fiducial value	Finite difference (h)
H	67.4	fiducial $\times 0.1$
$\Omega_b h^2$	0.0223	fiducial $\times 0.1$
$\Omega_c h^2$	0.119	fiducial $\times 0.005$
n_s	0.965	fiducial $\times 0.005$
A_s	2.13×10^{-9}	fiducial $\times 0.1$
τ	0.063	fiducial $\times 0.1$
m_ν	0.06	fiducial $\times 0.1$
w_0	-1	0.03

Table 4. Fiducial cosmological parameters and their finite-difference steps

To test the accuracy, we varied h by $\pm 5\%$ and $\pm 10\%$ and compared the relative change in the derivative of the equilateral lensing bispectra and the lensing powerspectra. As long as numerical noise doesn't dominate, it can be shown that the relative error in our approximation is approximately 5 times the relative difference that taking $h \to h(1 \pm 0.1)$ leads to. We thus conclude that, based on the tests conducted, the derivatives are almost always computed with up to one percent error. The exception is the derivative with respect to neutrino masses, which introduces a larger error of around 10 percent.

[10] As confirmed during a conversation with the author.

F ΛCDM constraints

We do not expect to use weak lensing surveys to competitively constrain the main ΛCDM parameters. Despite this, we include these constraints for completeness in figures 8, 9, 10, 11, and in table 5. All survey parameters are the same as in section 4.

weak priors										
		CMB lensing			Gal. lensing			CMB × Gal. lensing		
Par	prior	C_ℓ	$B_{\ell_1\ell_2\ell_3}$	$C_\ell + B_{\ell_1\ell_2\ell_2}$	C_ℓ	$B_{\ell_1\ell_2\ell_3}$	$C_\ell + B_{\ell_1\ell_2\ell_3}$	C_ℓ	$B_{\ell_1\ell_2\ell_3}$	$C_\ell + B_{\ell_1\ell_2\ell_3}$
H_0	17	17	16	6.5	13	4.2	1.8	1.6	1.5	1.0
$10^3\Omega_b h^2$	0.50	0.50	0.50	0.50	0.50	0.48	0.48	0.50	0.48	0.46
$\Omega_c h^2$	0.29	0.0070	0.012	0.0063	0.0095	0.0049	0.0041	0.0050	0.0044	0.0033
n_s	0.020	0.019	0.020	0.018	0.020	0.017	0.011	0.015	0.016	0.010
τ	0.063	0.063	0.063	0.063	0.063	0.063	0.063	0.063	0.063	0.063
$10^9 A_s$	1.0	0.36	0.91	0.30	0.53	0.10	0.10	0.081	0.098	0.063
CMB $T + E$ priors										
		CMB lensing			Gal. lensing			CMB × Gal. lensing		
Par	prior	C_ℓ	$B_{\ell_1\ell_2\ell_3}$	$C_\ell + B_{\ell_1\ell_2\ell_2}$	C_ℓ	$B_{\ell_1\ell_2\ell_3}$	$C_\ell + B_{\ell_1\ell_2\ell_3}$	C_ℓ	$B_{\ell_1\ell_2\ell_3}$	$C_\ell + B_{\ell_1\ell_2\ell_3}$
H_0	1.2	1.1	1.2	1.1	1.1	0.90	0.66	0.84	0.78	0.43
$10^3\Omega_b h^2$	0.057	0.053	0.057	0.053	0.056	0.053	0.052	0.051	0.052	0.050
$\Omega_c h^2$	0.00083	0.00076	0.00081	0.00076	0.00064	0.00068	0.00053	0.00048	0.00061	0.00043
n_s	0.0025	0.0025	0.0025	0.0025	0.0022	0.0024	0.0022	0.0020	0.0022	0.0018
τ	0.013	0.011	0.012	0.011	0.011	0.010	0.0093	0.0091	0.0098	0.0082
$10^9 A_s$	0.055	0.044	0.049	0.043	0.045	0.041	0.037	0.036	0.039	0.032

Table 5. Same as table 3, except for ΛCDM parameters.

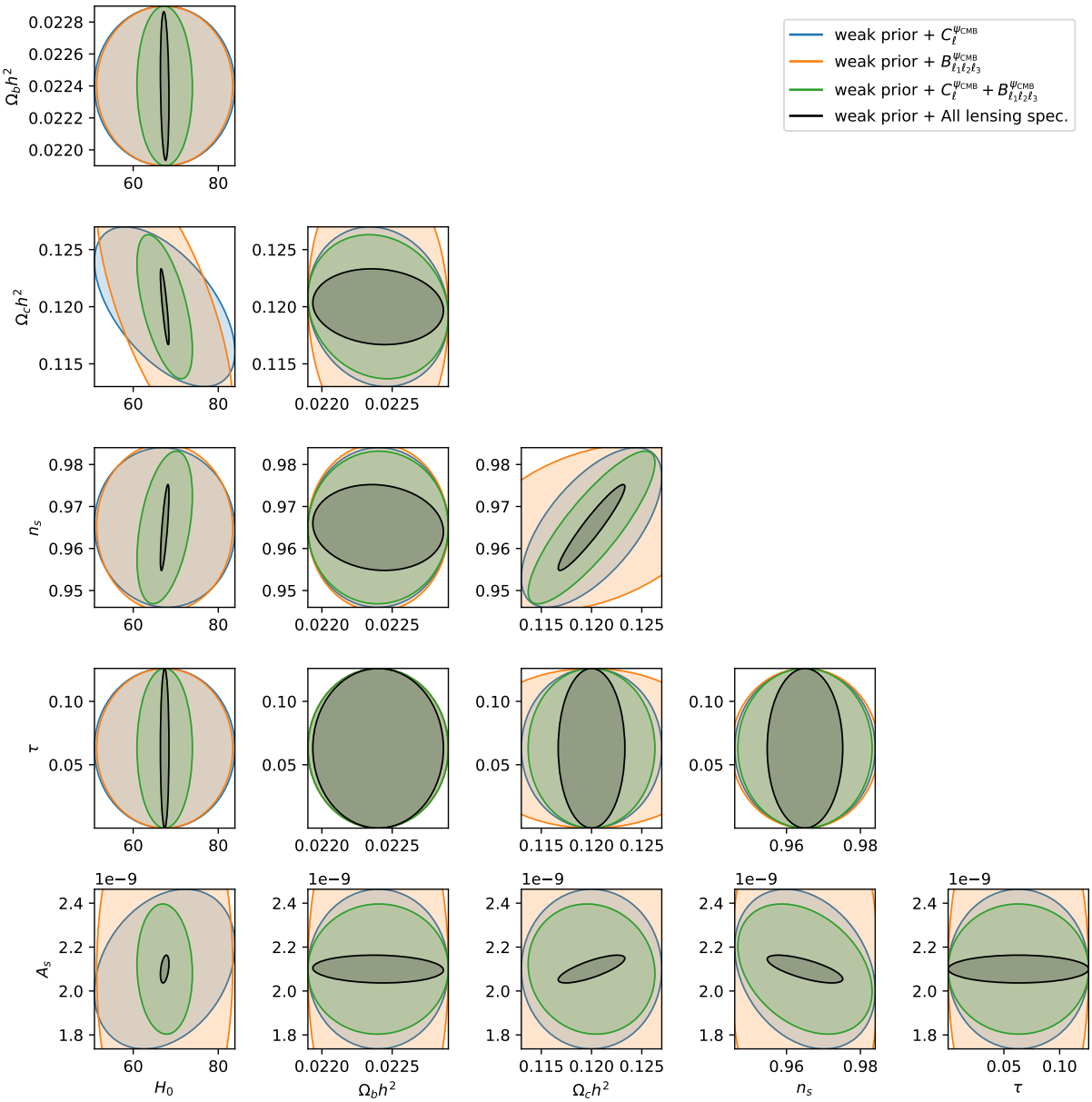

Figure 8. Same as figure 3, except for the standard ΛCDM parameters.

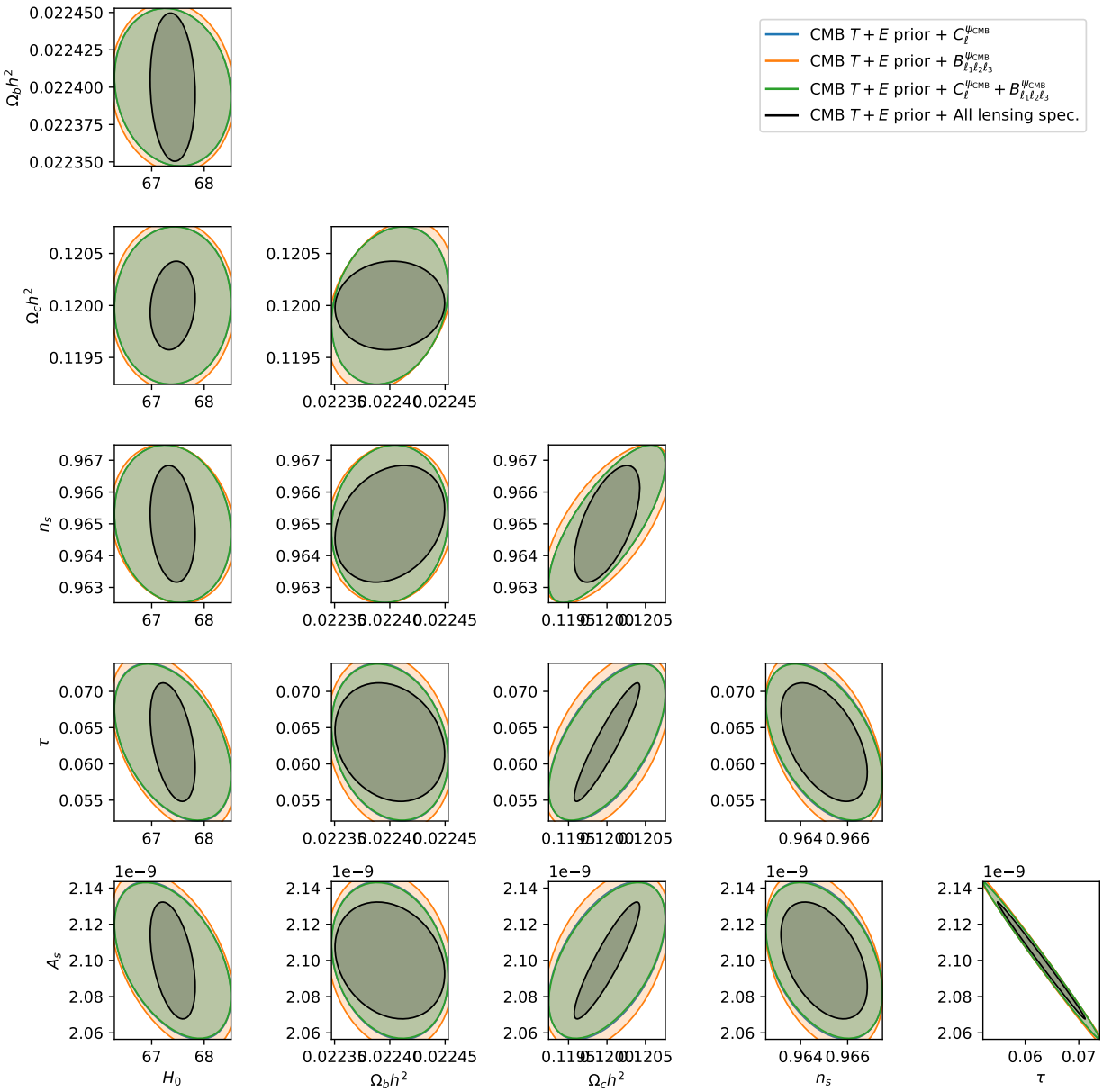

Figure 9. Same as figure 4, except for the standard ΛCDM parameters.

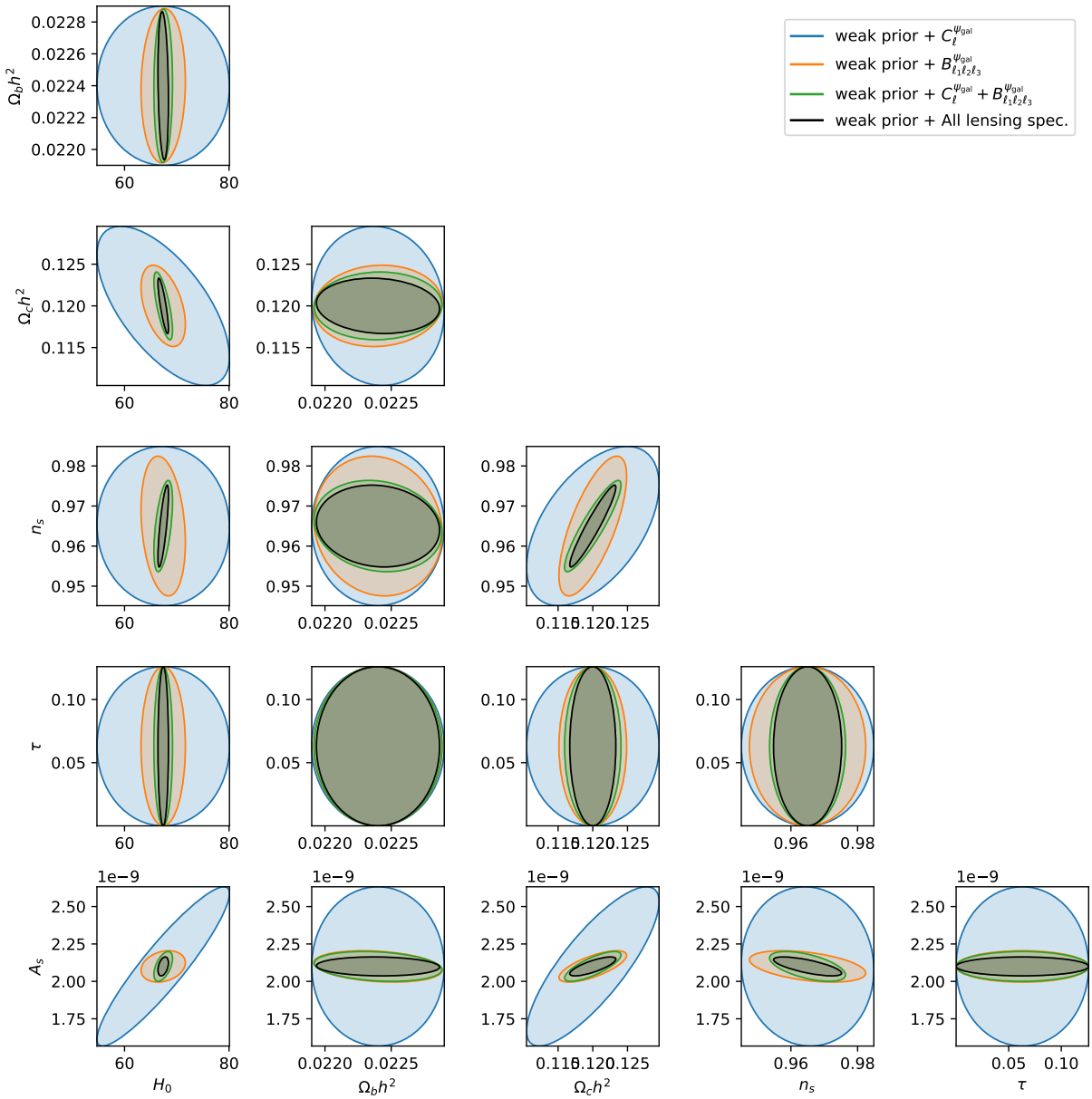

Figure 10. Same as figure 5, except for the standard ΛCDM parameters.

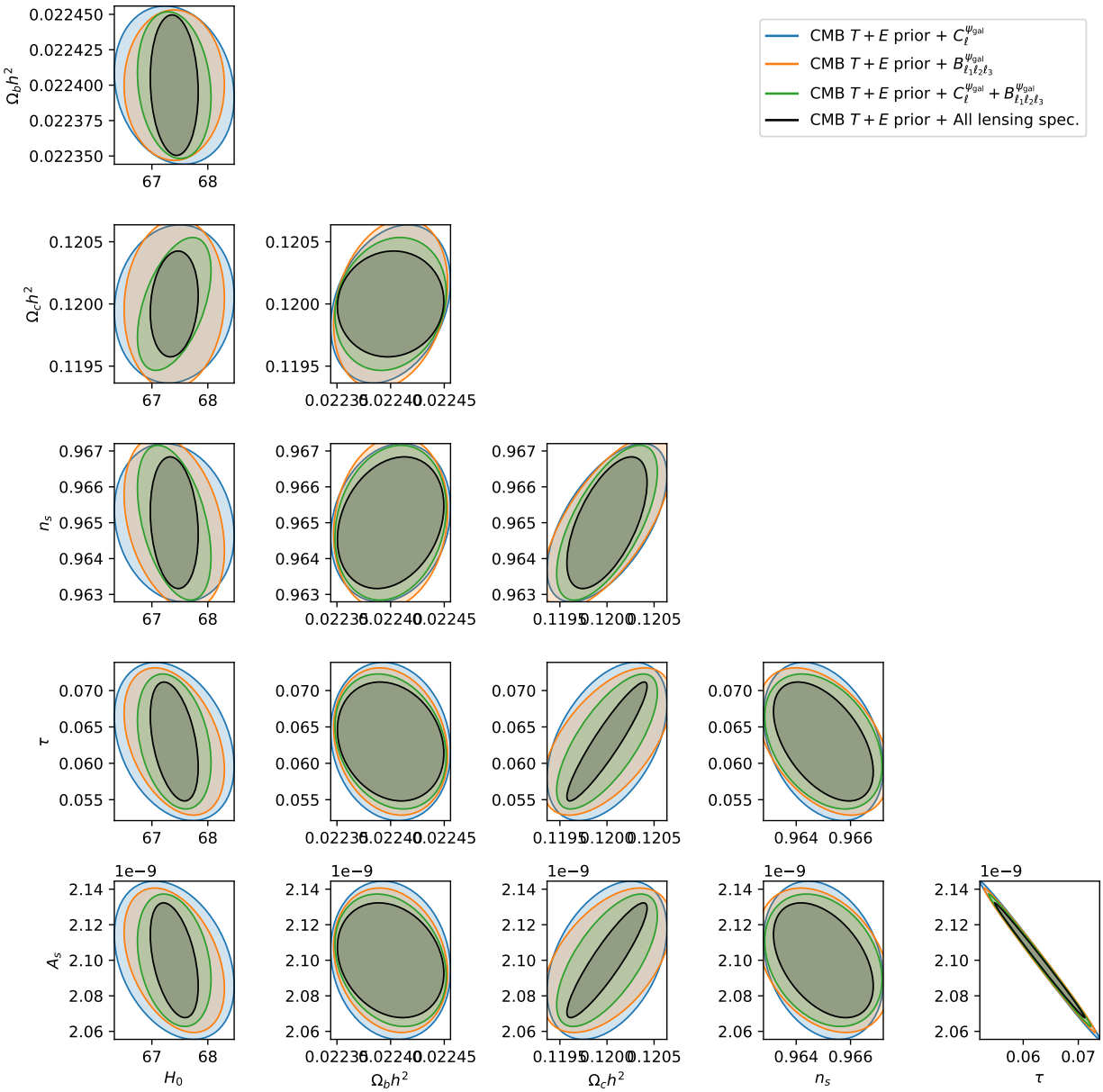

Figure 11. Same as figure 6, except for the standard ΛCDM parameters.